GEOLOGY

Pacific warm pool subsurface heat sequestration modulated Walker circulation and ENSO activity during the Holocene

Haowen Dang[1], Zhimin Jian[1]*, Yue Wang[1], Mahyar Mohtadi[2], Yair Rosenthal[3], Liming Ye[4], Franck Bassinot[5], Wolfgang Kuhnt[6]

Dynamics driving the El Niño–Southern Oscillation (ENSO) over longer-than-interannual time scales are poorly understood. Here, we compile thermocline temperature records of the Indo-Pacific warm pool over the past 25,000 years, which reveal a major warming in the Early Holocene and a secondary warming in the Middle Holocene. We suggest that the first thermocline warming corresponds to heat transport of southern Pacific shallow overturning circulation driven by June (austral winter) insolation maximum. The second thermocline warming follows equatorial September insolation maximum, which may have caused a steeper west-east upper-ocean thermal gradient and an intensified Walker circulation in the equatorial Pacific. We propose that the warm pool thermocline warming ultimately reduced the interannual ENSO activity in the Early to Middle Holocene. Thus, a substantially increased oceanic heat content of the warm pool, acting as a negative feedback for ENSO in the past, may play its role in the ongoing global warming.

INTRODUCTION

The equatorial eastern Indian and western Pacific oceans with a persistent sea surface temperature (SST) above 28°C [termed the Indo-Pacific warm pool (IPWP)] represent a major oceanic heat source for the atmosphere, characterized by deep atmospheric convection accompanied with heavy rainfall (*1*). The heat storage in the IPWP is essentially formed by the accumulation of warm surface waters driven by the equatorial trade winds (*2*) and modulated by the convergence of subsurface ocean heat anomalies from North and South subtropical and eastern Pacific (Fig. 1A) (*3*). The west-east (W-E) thermal asymmetry across the tropical Pacific and associated Walker circulation play a key role in both the interannual variability of El Niño–Southern Oscillation (ENSO) (*2*, *4*) and the decadal to multidecadal Pacific climate changes (*3*, *4*, *5*). In association with the greenhouse warming over the 20th century, the equatorial Pacific W-E thermal gradient was possibly reduced, the Walker circulation slowed down (*6*), and the ENSO variability increased (*4*, *7*). More recently, the slowdown of surface air warming between ~2000 and 2014 AD (aka "global warming hiatus") was featured by substantial cooling of equatorial Pacific SST and strengthening of the zonal thermal gradient and the Walker circulation (*3*, *5*), which has been attributed to enhanced heat storage in the equatorial Pacific thermocline (*8*, *9*). It is not fully resolved, however, over decadal and even longer time scales, how the upper-ocean heat anomalies will vary with changes in the Walker circulation, ENSO activity, and the shallow overturning circulation from the subtropics. Understanding these relationships can greatly improve the prediction of the future climate change.

On longer time scales, from the Last Glacial Maximum [LGM; 19 to 25 ka (kilo annum, thousand years before 1950 AD)] to the Early Holocene (9 to 12 ka), a warming of up to 4°C has been observed in the thermocline temperature records over the IPWP (*10*, *11*, *12*), possibly leading to a reduction of ENSO activity in the Early to Middle Holocene (*13*, *14*). In addition, stalagmite records from Borneo suggest that Walker circulation was relatively weak during the last deglacial and strengthened in the Middle Holocene (4 to 7 ka) (*15*) when ENSO activity was suppressed (*16*). However, while the Borneo stalagmite record suggests similar-to-modern ENSO activity during the Early Holocene (*16*), other proxy records of ENSO activity from eastern equatorial Pacific indicate little or no ENSO activity during this period (*17*, *18*). Such a discrepancy is largely caused by the sparsity of sedimentary archives and thus leads to an incomplete understanding of past changes in the upper-ocean heat structure of the IPWP.

Here, we present a compilation of more than 30 sedimentary proxy records (3 from this work) from the equatorial Pacific (Fig. 1A and table S1) to comprehensively examine changes in the upper-water (thermocline and above) temperature of the IPWP over the past ~25,000 years. We excluded five records [e.g., those from southwest Sumatra (*19*)] that are predominately influenced by local processes such as upwelling and do not reflect the general characteristics of IPWP's subsurface (table S1). The records with an average temporal resolution of ~150 years constrained by a total of 217 radiocarbon dates (see Materials and Methods and table S2) covering the course of the LGM through the Holocene. The thermal structure of IPWP is examined by reconstructing temperatures of the thermocline water (TWT) and sea surface (SST) using shell Mg/Ca of two planktic foraminifera, the upper-thermocline dweller *Pulleniatina obliquiloculata* (*20*, *21*) and the mixed-layer dweller *Globigerinoides ruber* (see Materials and Methods) (*21*). To minimize the possible interlaboratory and intercalibration biases and the effect of different cleaning protocols (see the Supplementary Materials), we calculated

[1]State Key Laboratory of Marine Geology, Tongji University, Shanghai 200092, China. [2]MARUM-Center for Marine Environmental Sciences, University of Bremen, 28359 Bremen, Germany. [3]Department of Marine and Coastal Science and Department of Earth and Planetary Sciences, Rutgers University, New Brunswick, NJ 08901, USA. [4]Key Laboratory of Submarine Geosciences, Second Institute of Oceanography, Ministry of Natural Resources of China, Hangzhou 310012, China. [5]Laboratoire des Sciences du Climat et de l'Environnement/IPSL, CEA-CNRS-UVSQ, University Paris-Saclay, 91198 Gif-sur-Yvette, France. [6]Institute of Geosciences, Christian-Albrechts-University, D-24118 Kiel, Germany.
*Corresponding author. Email: jian@tongji.edu.cn

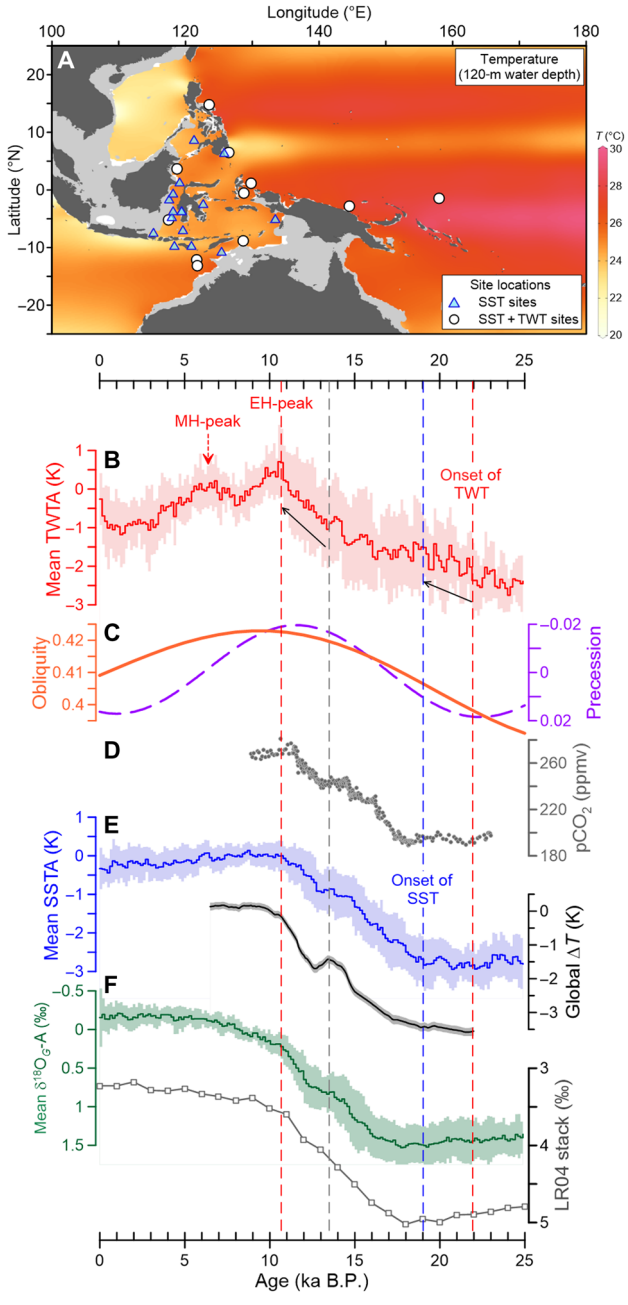

Fig. 1. Time series of thermocline and SST anomalies in the IPWP compared to global climate indices during the past 25,000 years. (**A**) Site locations of paired SST and thermocline water temperature (TWT) records (white circles) and SST-only records (blue triangles) (table S1). Shadings indicate temperatures at 120-m water depth. (**B**) Mean TWTA (red) of the IPWP records. Solid black arrows mark the two major warming phases of TWTA between 22 to 19 ka and 13 to 11 ka, respectively. (**C**) Precession (dashed purple) and obliquity (orange) parameters (*47*). (**D**) Atmospheric pCO_2 derived from West Antarctic Ice Sheet Divide ice core [gray dots; (*26*)]. ppmv, parts per million by volume. (**E**) Mean SSTA (blue) of the IPWP records and the global mean SST anomaly [ΔT, dark gray line; (*48*)]. (**F**) Mean IPWP *G. ruber* $\delta^{18}O_G$ anomaly ($\delta^{18}O_G$-A, green) and LR04 benthic $\delta^{18}O$ stack [gray line and symbols; (*49*)]. Shadings of proxy records show the 1σ SD. Vertical dashed lines denote the timing of the deglacial onset of SST (~19 ka, blue) and TWT (~22 ka, red), the onset of the second deglacial warming step (gray), and the Early Holocene peak of TWT (EH-peak, ~10.8 ka, red). Dotted red arrow denotes the Middle Holocene peak of TWT (MH-peak, 7 ka). B.P., before the present.

the SST and TWT anomalies relative to the average value of each temperature record over 6 to 10 ka (denoted as SSTA and TWTA; Fig. 1, B and D). The records of *G. ruber* $\delta^{18}O$ from 22 cores are processed in the same way to acquire the mean $\delta^{18}O_{G.\ ruber}$ anomaly ($\delta^{18}O_G$-A; Fig. 1F) and are calculated for seawater $\delta^{18}O$ by subtracting the amount related to changes in local temperature and global ice volume [see the Supplementary Materials (*22*)]. Three deep thermocline temperature records of the eastern equatorial Pacific, estimated by the shell Mg/Ca of *Neogloboquadrina dutertrei*, are also analyzed (table S1).

RESULTS

Mean TWTA and SSTA variations

The mean SSTA continuously warms by ~2.8° ± 0.6°C since ~19 to ~10 ka and cools by ~0.3° ± 0.5°C from ~9 to 0 ka (Fig. 1E), consistent with previous estimates (*23*, *24*). The deglacial onset of positive SSTA occurs at ~18 ka with site-specific differences (*25*), which is generally synchronous with the onsets of the atmospheric pCO_2 rise (Fig. 1D), global mean SST warming (Fig. 1E), and decreases in the IPWP mean *G. ruber* $\delta^{18}O$ and the global benthic $\delta^{18}O$ stack (Fig. 1F).

The mean TWTA warms by 3.0° ± 0.6°C from ~22 to 11 to 9 ka and cools by 1.0° ± 0.7°C from 9 to 0 ka (Fig. 1B). The TWTA at 11 to 9 ka is highest and synchronous with the precession minimum and obliquity maximum (Fig. 1C). The onset of deglacial warming occurs at ~22 ka in TWTA, in phase with the turning point of precession parameter (Fig. 1C) and precedes the deglacial pCO_2 rise (*26*) by ~4000 years (Fig. 1D). The deglacial mean TWTA warming mainly occurs in two phases: a first warming between 22 and 19 ka, coeval with the initial decrease of precession parameter, and a second warming between 13 and 11 ka, coinciding with the minima of precession parameter (Fig. 1B). The later warming phase is also synchronous with the final phase in the deglacial rise of the atmospheric pCO_2 (Fig. 1D). The overall trend and the timing of the deglacial warming illustrate that orbital-driven insolation forcing controls the TWT change in the IPWP.

Besides the warm TWTA peak at ~11 ka, a second peak is found around 7 to 6 ka (Fig. 1B). TWT features observed in sites from open ocean differ from those within the Maritime Continent waters. The TWTA from open-ocean sites gradually warms from 22 ka and peaks at 11 to 10 ka (Fig. 2A), which we define as the Early Holocene peak (EH-peak) type. The near-equator TWTA records from the Maritime Continent waters are characterized by a rise after 15 ka and a Middle Holocene warm peak around 7 ka (Fig. 2B), defined as the Middle Holocene peak (MH-peak) type. The principal components analysis confirms the distinction, with a first principal component (Fig. 2C) yielding positive loadings for all records (Fig. 2D) and a second principal component (Fig. 2C) yielding different signs of loadings among the sites (Fig. 2E). The linear combinations of the first and second principal components resemble the two types of TWTA change (Fig. 2F), suggesting that "PC1 – PC2" represents the feature of EH-peak type TWTA and "PC1 + PC2" represents the MH-peak type.

The Early Holocene TWTA peak

The EH-peak type, consistent with the mean TWTA trend (Fig. 1B), is in phase with the changes in Earth's orbital configuration of precession and obliquity (Fig. 3A). The relationship between precession/obliquity

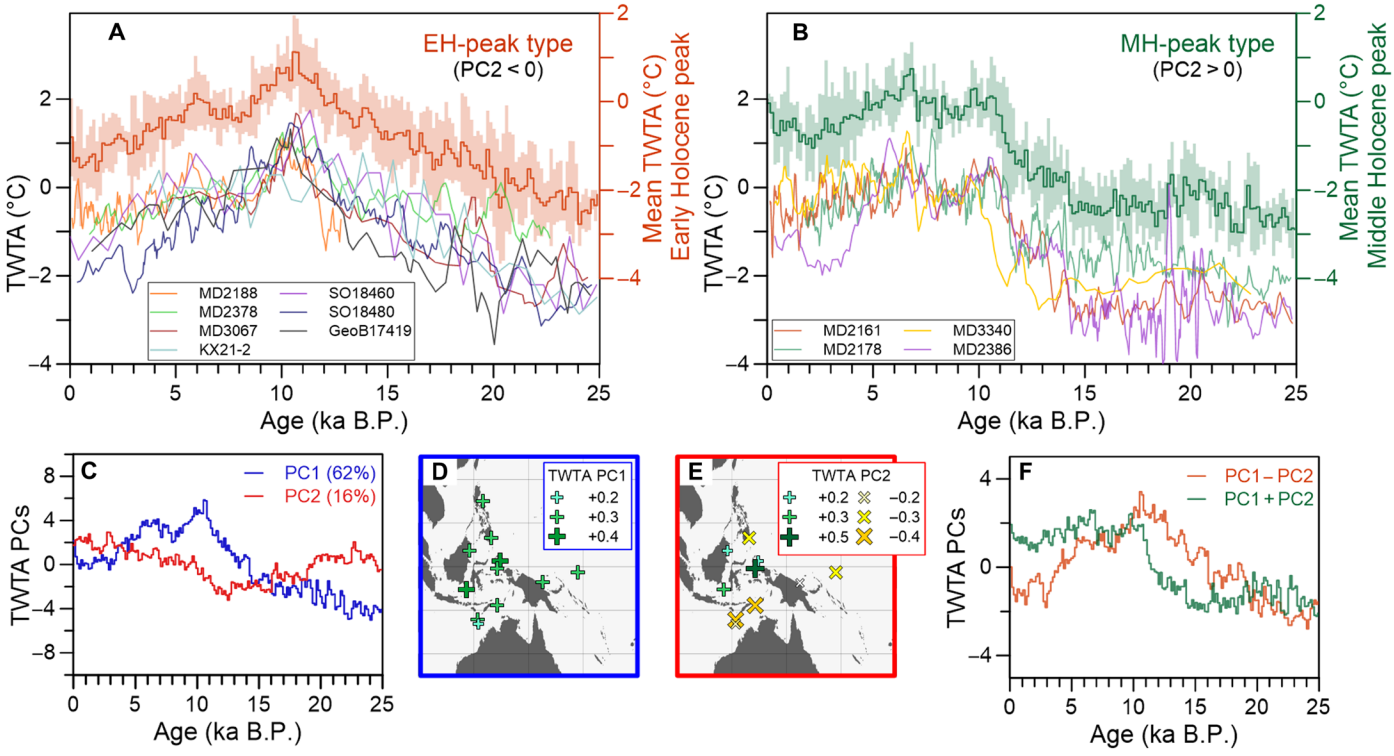

Fig. 2. The two types of thermocline temperature anomaly (TWTA) records in the IPWP since the LGM. (**A**) Average TWTA (brown) and the original TWTA records of the open-ocean sites. (**B**) Same as (A) but for the near-equator sites in the Maritime Continent waters. The TWT records in (A) and (B) are defined as (EH-peak and MH-peak types), respectively. (**C**) First (blue) and second (red) principal components (PCs) of all the TWTA records. PC1 and PC2 explain 62 and 16% of the total variance, respectively. (**D** and **E**) Loadings of PC1 (D) and PC2 (E) for each site. (**F**) Linear combinations of PC1 and PC2 that resemble the Early Holocene peak type (PC1 − PC2) and Middle Holocene peak type (PC1 + PC2), respectively.

and IPWP's thermocline change has been found before (*10*–*12*, *27*, *28*) and was explained by some regional oceanographic processes. Such a common Early Holocene peak, however, implies a common driving mechanism over the entire IPWP thermocline. The western equatorial Pacific thermocline water originates from the basin-wide shallow overturning circulation of the Pacific Ocean (*1*, *29*), which is fed by the subduction of relatively salty, warm surface waters in the subtropical North and South Pacific (*1*), and is primarily regulated by the surface wind stress curls determined by the meridional SST gradients (*30*). Over the past 25 ka, the gradient between the southwestern Pacific SSTA (from 45.5°S, 174.9°E) (*31*, *32*) and the IPWP mean SSTA (Fig. 3B) resembles the EH-peak type TWTA, possibly reflecting relatively warmer midlatitude and thereby enhanced warm water transport of shallow overturning circulation in the Early Holocene. In addition, foraminifera $\delta^{13}C$ records of the equatorial Pacific also suggest an Early Holocene intensification in the advection of southern-sourced subsurface waters (*33*, *34*). An Early Holocene peak also appears in the southern Pacific and Antarctic temperature records because of the June (austral winter) insolation maximum at precession minimum (fig. S3). In modern observations (*35*), the northern Pacific shallow overturning circulation also contributes to the IPWP thermocline water, but the northwestern Pacific SSTA record shows no direct linkage to the Early Holocene peak in IPWP thermocline (fig. S3). Therefore, we can only propose that the overall trend of IPWP's thermocline evolution over the LGM-Holocene may be dominated by the southern Pacific shallow overturning circulation, under the control of changing meridional insolation gradient induced by orbital forcing [i.e., precession and obliquity (*36*)].

Our hypothesized mechanism for the Pacific subsurface temperature change is verified by a transient simulation of the Community Earth System Model [CESM1.0.4 (*37*)], forced by the orbital insolation and greenhouse gas (GHG) changes of the past 300,000 years (detailed in Materials and Methods)(*38*). The responses of the Pacific upper-ocean thermal structure point out the key role played by precession in forming the Early Holocene peak of TWT in the IPWP. At precession minimum during the Early Holocene, an intrusion of southern Pacific warm waters resulted in a drastic thermocline warming in the 30- to 200-m water depth of the open-ocean equatorial Pacific (140°E to 140°W; Fig. 3, C to E) and in the relatively deeper (below 120-m water depth) Maritime Continent waters (100°E to 140°E; Fig. 3F) (*39*). Noteworthy, the precession minimum also induces considerable cooling anomalies in the shallower Maritime Continent waters above 120-m depth in our simulation (Fig. 3F), in contrast to the paleo-proxy–based Early Holocene TWTA warming off the Philippines and in the Timor Sea. Therefore, the Early Holocene TWT warming in the IPWP may be a result of the precession-forced warming of deeper thermocline waters (Fig. 3D), which cannot be explained by the obliquity maximum with a cooling effect instead (fig. S4). Of course, the Early Holocene warming may also be induced by the influence of increased atmosphere pCO_2, which results in a universal warming at all latitudes

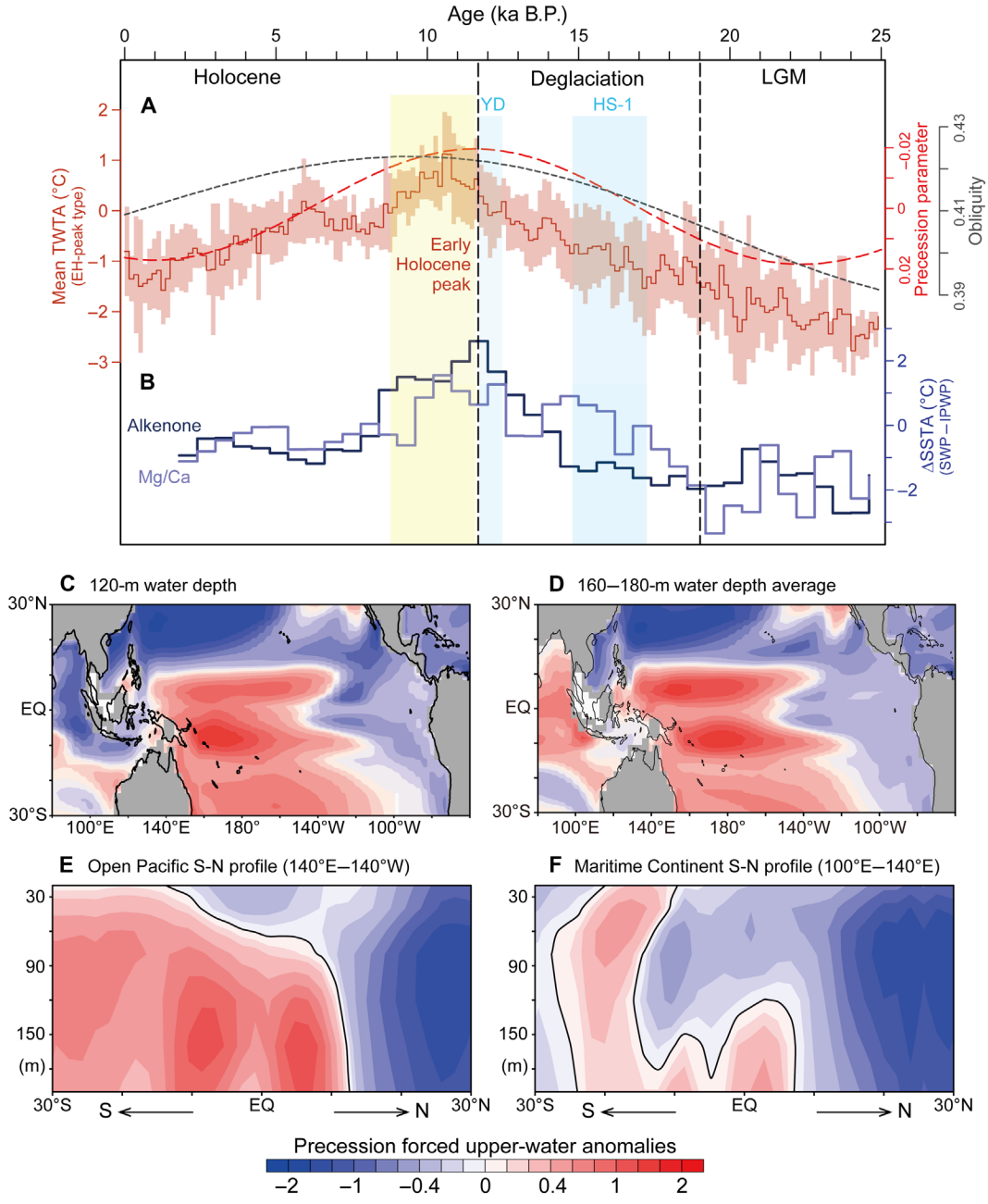

Fig. 3. Precession-forced Early Holocene TWTA peak. (**A**) Mean TWTA of the Early Holocene peak type (brown), precession (red dashed line), and obliquity [gray dashed line; (*47*)]. (**B**) Meridional SSTA gradient between southwest Pacific [SWP; site MD97-2120, from 45.5°S, 174.9°E; (*31*–*32*)] and the IPWP. Holocene, last deglaciation, and LGM are separated by dashed vertical lines. CESM-simulated responses of Pacific subsurface temperature to June insolation in the Early Holocene are shown in (**C** to **F**): horizontal temperature anomaly distributions of upper-thermocline [at 120 m in (C)] and deeper thermocline [160- to 180-m water depth average in (D)] and meridional upper-water temperature anomaly profiles in the open Pacific [140°E to 140°W in (E)] and the Maritime Continent waters [100°E to 140°E in (F)]. Temperature anomalies in (C) to (F) are shown as regression coefficients against the standardized time series of the June insolation at precessional band in experiment CESM_GHG. White shadings mask insignificant results below 95% confidence level (*t* test). EQ, equator.

(fig. S4). In addition, the deglacial sea level rise can also deepen the thermocline and result in thermocline warming in the Maritime Continent waters (*40*). Thus, the Early Holocene warming of the IPWP subsurface water could have been caused by the combined effect of precession minimum, atmosphere pCO_2 maximum, and sea level high stand.

The Middle Holocene TWTA peak

For the near-equator sites within the Maritime Continent waters, the most substantial thermocline warming occurs in the Middle Holocene. These records share two main features: (i) a cooling spell in 18 to 15 ka and (ii) a warming peak at ~7 ka (Fig. 4A). These sites are apparently less directly influenced by the southern Pacific

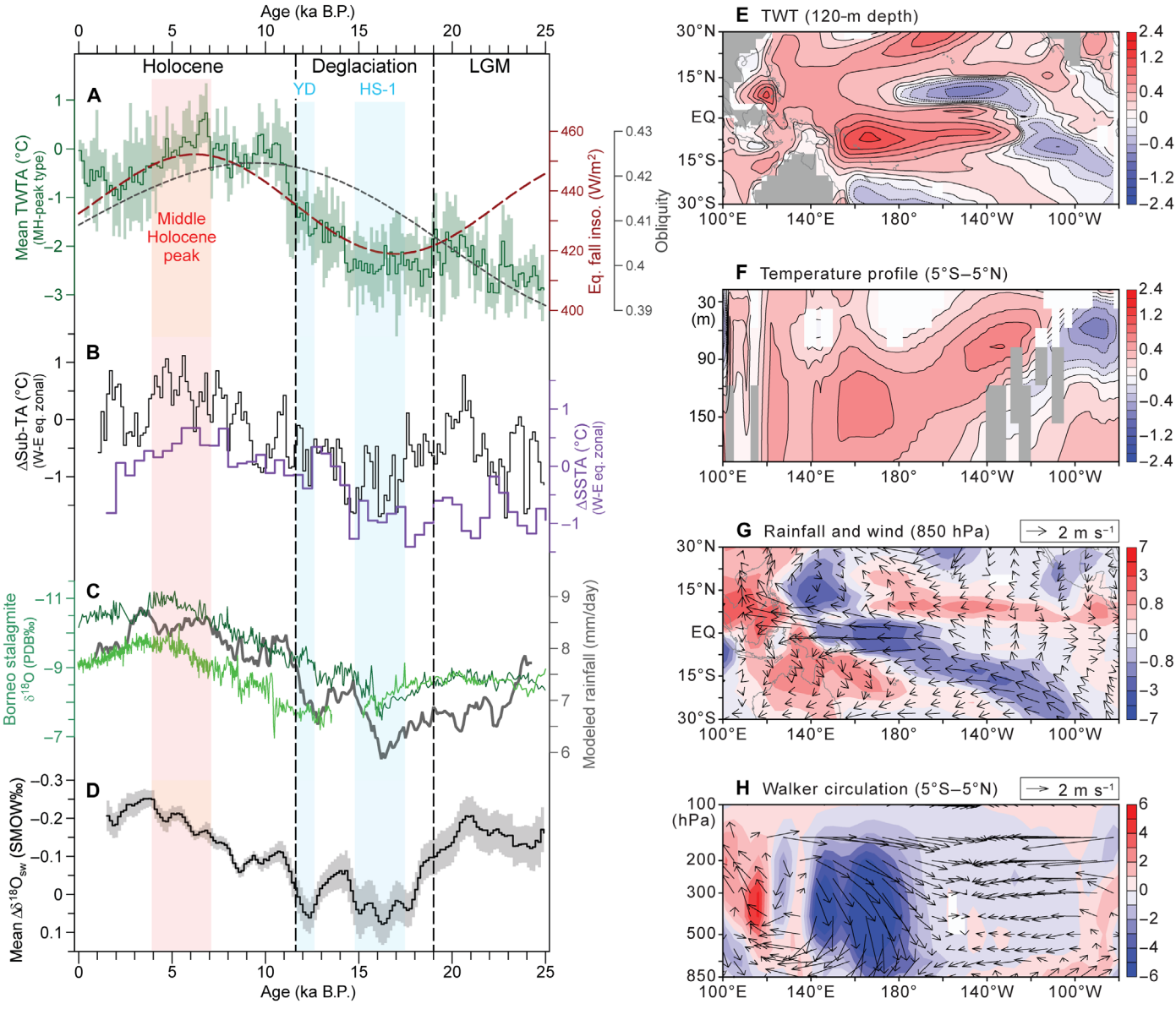

Fig. 4. Time series and simulated temperature and rainfall anomalies in the IPWP since the LGM. (**A**) Mean TWTA of Middle Holocene peak type (green) and the September 21st insolation at the equator (dashed red line) and obliquity [gray dotted line; (*47*)]. (**B**) Zonal temperature gradients at subsurface (Δsub-TA, in gray) and at sea surface [ΔSSTA, in violet; (*42*)] shown as the difference between the western equatorial Pacific and eastern equatorial Pacific. (**C**) $\delta^{18}O$ records of northern Borneo stalagmites (*15*, *16*) (dark and light green) and simulated annual mean rainfall (millimeters per day) over Borneo (dark gray, this study). PDB, Pee Dee belemnite. (**D**) Mean anomaly of seawater $\delta^{18}O$ of IPWP ($\Delta\delta^{18}O_{sw}$, dark gray, shading shows the 1σ error of the records). Shadings, vertical bars, and dashed lines are as in Fig. 3. Simulated response of the Pacific subsurface temperature and atmospheric variables to September insolation maximum are shown in (**E** to **H**): (E) Annual mean TWTA at 120-m water depth. (F) Depth profile of the annual mean temperature anomaly across the Pacific between 5°S and 5°N. (G) Late-autumn (October to December) anomalies of mean rainfall (colors, in millimeters per day) and horizontal winds at 850 hPa (arrows, in meters per second, reference arrow on top right). (H) Late-autumn mean Walker circulation anomalies between 5°S and 5°N across the Pacific, as indicated by anomalies in wind (arrows, in meters per second, reference arrow on top right) and in vertical velocity (colors, in pascal per second). Positive values in red indicate upward motion, and negative values in blue indicate downward motion. These anomalies in (E) to (H) are shown as regression coefficients against the standardized time series of the September insolation at precessional band in experiment CESM_GHG. SMOW, standard mean ocean water.

sourced signal of the Early Holocene TWTA peak. The MH-peak type TWTA varies in phase with the equatorial September insolation change (Fig. 4A) that dominates ENSO-related activities in the tropical Pacific (*41*). For example, the overall pattern of the MH-peak type TWTA is consistent with the W-E zonal temperature difference in both the sea surface (*42*) and subsurface across the equatorial Pacific, which shows maxima in the Middle Holocene and minima in the early stage of the deglaciation (Fig. 4B). Likewise, the strength of the ascending limb of the Walker circulation, as indicated by the Borneo stalagmite $\delta^{18}O$ records, shows a

minimum (more positive $\delta^{18}O$) around 17 to 16 ka and a maximum (more negative $\delta^{18}O$) around 7 ka (Fig. 4C), suggesting an enhanced atmospheric convection over Borneo in the Middle Holocene.

The hydroclimate changes revealed by Borneo stalagmite are supported by our CESM simulation of annual mean rainfall time series over Borneo forced solely by orbital insolation change (Fig. 4C). In addition to the Borneo stalagmite records, the surface seawater $\delta^{18}O$ stack ($\delta^{18}O_{sw}$) of the IPWP shows positive excursions in the last deglacial and a negative peak in the Middle Holocene (Fig. 4D), indicating a strengthened convective precipitation over evaporation in the Middle Holocene. Thus, we argue that the Middle Holocene thermocline warming of the near-equator IPWP is dynamically linked to the equatorial Pacific ENSO-like changes (e.g., enhanced Walker circulation and strengthened W-E zonal thermal contrast in the Middle Holocene). Our model simulations verify that September insolation maximum forces a warming in the IPWP thermocline (Fig. 4E) and a stronger zonal thermal difference across the equatorial Pacific (Fig. 4F). The atmospheric response to an increased zonal thermal gradient leads to increased rainfall over western equatorial Pacific (Fig. 4G) and a stronger Walker circulation (Fig. 4H).

DISCUSSION

The long-term evolution of the tropical Pacific mean state—including the IPWP's thermocline temperature, the W-E temperature gradients, and the western equatorial Pacific hydroclimate—has the potential to shape shorter-term climate oscillations, i.e., interannual ENSO activity, as suggested by simple model simulations (*41*, *43*). An Early to Middle Holocene depression of ENSO activity associated with strengthening of the Walker circulation relative to modern is evidenced by several proxy records and model simulations (*13*, *16*, *44*). Our findings suggest that the evolution of the equatorial Pacific climate in response to precession forcing could be understood in analogy to the modern seasonal development of the equatorial Pacific air-sea coupled system (*2*). That is, in the Early Holocene under the precession minimum, the thermocline of the open-ocean IPWP warmed widely, thereby likely suppressing ENSO activity. During the Middle Holocene, maximal September insolation may have caused an overall thermocline warming, increased precipitation, and decreased sea surface salinity in the IPWP and strengthening of the Walker circulation (Fig. 4D). A maximum in W-E upper-ocean thermal contrast (Fig. 4B) ultimately led to an extreme reduction of ENSO activity in the Middle Holocene.

The response of ENSO activity to future global warming and consequences to Earth's climate evolution are not well constrained by either modern observations or model simulations (*45*), thus necessitating additional observations from paleoclimate records. Our study shows that warming of the western equatorial Pacific thermocline coupled with increased W-E thermal gradient and strengthened Walker circulation may have ultimately led to the reduction in ENSO activity during the Early and Middle Holocene, when climate was arguably slightly warmer than at present (*39*, *46*). This inference raises the possibility that enhanced anthropogenic heat sequestration in the western equatorial Pacific subsurface waters, through the shallow overturning cell and equatorial Pacific air-sea coupled system, may further augment heat uptake in the eastern equatorial Pacific cold tongue due to reduced ENSO activity. In the near future, these may subsequently lead to an intermittent slowdown of surface warming, likely for short periods, in a pattern akin to the global warming hiatus between 2000 and 2014 (*3*, *5*, *9*).

MATERIALS AND METHODS

We analyzed the Mg/Ca and $\delta^{18}O$ of *G. ruber* (250 to 350 μm) and *P. obliquiloculata* (350 to 440 μm) at the State Key Laboratory of Marine Geology, Tongji University, Shanghai, China. Mg/Ca measurements were conducted on an inductively coupled plasma mass spectrometry (Thermo VG-X7) with a measurement reproductivity of 2.2% for *G. ruber* ($n = 311$) and 4.8% for *P. obliquiloculata* ($n = 302$), estimated by replicate samples (n, total replicates of the three cores of this study; for details, see table S2). The shell $\delta^{18}O$ of the two species was measured with a Finnigan-MAT253 mass spectrometer. Conversion to the international Pee Dee belemnite scale was performed using NBS19 standard, and the long-term variability of $\delta^{18}O$ is better than 0.07 per mil. Details of pretreatments and procedures are described elsewhere (*20*).

The age models for the IPWP cores were all established mainly by linear relationships of radiocarbon dates, first corrected for the ^{14}C reservoir ages by the Marine Reservoir Correction and then calibrated to calendar age using CALIB7.1 software (http://calib.org) (tables S1 and S3). The time series of proxies (SST, TWT, and $\delta^{18}O$) were then averaged at 150-year nonoverlapping bins using the staircase integration resampling method. The temperature gradients of IPWP relative to the eastern equatorial Pacific or extratropical seas are calculated by the differences between the respective temperature anomaly records and on temporal steps determined by the average temporal resolution of the corresponding records (150 years for W-E subsurface temperature gradient, 500 years for W-E SST gradient, and 600 years for South-Equatorial Pacific SST gradient).

Here, we use the CESM1.0.4 with T31_gx3v7 resolution [3.75° × 3.75° for atmosphere and nominal 3° resolution for ocean (*37*)] to simulate the response of Pacific upper-ocean thermal structure to the forcing of orbital configuration (obliquity and precession) and change in atmospheric GHG content (*38*). As a spin-up, the CESM was first run for 200 model years under orbital parameters and GHG of 300 ka and other boundary conditions in 1950 AD. Then, the model was integrated for 3000 model years with the transient orbital insolation forcing and GHG changes of the past 300,000 years, in which orbital parameters and GHG were advanced by 100 years at the end of each model year (experiment CESM_GHG). A similar transient accelerated experiment (CESM_ORB) was only forced by orbital insolation changes since 300 ka (*38*). The outputs in the last 3000 model years of these two experiments were both analyzed, and they exhibit similar responses to orbital insolation forcing. Thus, only the results from experiment CESM_GHG are shown. At first, ocean temperature, salinity, atmospheric circulation, and precipitation are extracted from original outputs along multiple profiles [i.e., the latitude-longitude profile at 120-m water depth, the longitude-vertical profile along the equator, and the latitude-vertical profile zonally averaged over the open Pacific (140°E to 140°W) or the western Pacific (100°E to 140°E)]. Then, these oceanic and atmospheric variables were linearly regressed onto the normalized time series of specific orbital forcing [i.e., obliquity parameter changes, GHG changes, and the June or September insolation changes defined by the solstice or equinox precessional mode, respectively (*38*)]. Associated regression coefficients represent the Pacific air-sea coupled responses between the maxima and minima

of each orbital forcing. Statistical significance is assessed by the 95% confidence level of *t* test.

SUPPLEMENTARY MATERIALS

Supplementary material for this article is available at http://advances.sciencemag.org/cgi/content/full/6/42/eabc0402/DC1

REFERENCES AND NOTES

1. D. Gu, S. G. H. Philander, Interdecadal climate fluctuations that depend on exchanges between the tropics and extratropics. *Science* **275**, 805–807 (1997).
2. A. Timmermann, S.-I. An, J.-S. Kug, F.-F. Jin, W. Cai, A. Capotondi, K. M. Cobb, M. Lengaigne, M. J. McPhaden, M. F. Stuecker, K. Stein, A. T. Wittenberg, K.-S. Yun, T. Bayr, H.-C. Chen, Y. Chikamoto, B. Dewitte, D. Dommenget, P. Grothe, E. Guilyardi, Y.-G. Ham, M. Hayashi, S. Ineson, D. Kang, S. Kim, W. M. Kim, J.-Y. Lee, T. Li, J.-J. Luo, S. M. Gregor, Y. Planton, S. Power, H. Rashid, H.-L. Ren, A. Santoso, K. Takahashi, A. Todd, G. Wang, G. Wang, R. Xie, W.-H. Yang, S.-W. Yeh, J. Yoon, E. Zeller, X. Zhang, El Niño–Southern oscillation complexity. *Nature* **559**, 535–545 (2018).
3. S. McGregor, A. Timmermann, M. F. Stuecker, M. H. England, M. Merrifield, F.-F. Jin, Y. Chilkamoto, Recent Walker circulation strengthening and Pacific cooling amplified by Atlantic warming. *Nat. Clim. Change* **4**, 888–892 (2014).
4. W. Cai, L. Wu, M. Langaigne, T. Li, S. McGregor, J.-S. Kug, J.-Y. Yu, M. F. Stuecker, A. Santoso, X. Li, Y.-G. Ham, Y. Chikamoto, B. Ng, M. J. McPhaden, Y. Du, D. Dommenget, F. Jia, J. B. Kajtar, N. Keenlyside, X. Lin, J.-J. Luo, M. Martín-Rey, Y. Ruprich-Robert, G. Wang, S.-P. Xie, Y. Yang, S. M. Kang, J.-Y. Choi, B. Gan, G.-I. Kim, C.-E. Kim, S. Kim, J.-H. Kim, P. Chang, Pantropical climate interactions. *Science* **363**, eaav4236 (2019).
5. M. H. England, S. McGregor, P. Spence, G. A. Meehl, A. Timmermann, W. Cai, A. S. Gupta, M. J. McPhaden, A. Purich, A. Santoso, Recent intensification of wind-driven circulation in the Pacific and the ongoing warming hiatus. *Nat. Clim. Change* **4**, 222–227 (2014).
6. Z. Liu, Z. Jian, C. J. Poulsen, L. Zhao, Isotopic evidence for twentieth-century weakening of the Pacific Walker circulation. *Earth Planet. Sci. Lett.* **507**, 85–93 (2019).
7. W. Cai, G. Wang, B. Dewitte, L. Wu, A. Santoso, K. Takahashi, Y. Yang, A. Carréric, M. J. McPhaden, Increased variability of eastern pacific El Niño under greenhouse warming. *Nature* **564**, 201–206 (2018).
8. N. Ramesh, R. Murtugudde, All flavours of El Niño have similar early subsurface origins. *Nat. Clim. Change* **3**, 42–46 (2013).
9. R. Neale, J. Slingo, The Maritime Continent and its role in the global climate: A GCM study. *J. Climate* **16**, 834–848 (2003).
10. J. Xu, A. Holbourn, W. Kuhnt, Z. Jian, H. Kawamura, Changes in the thermocline structure of the Indonesian outflow during Terminations I and II. *Earth Planet. Sci. Lett.* **273**, 152–162 (2008).
11. T. Bolliet, A. Holbourn, W. Kuhnt, C. Laj, C. Kissel, L. Beaufort, M. Kienast, N. Andersen, D. Garbe-Schrönberg, Mindanao Dome variability over the last 160 kyr: Episodic glacial cooling of the West Pacific Warm Pool. *Paleoceanography* **26**, PA1208 (2011).
12. H. Dang, Z. Jian, F. Bassinot, P. Qiao, X. Cheng, Decoupled Holocene variability in surface and thermocline water temperatures of the Indo-Pacific Warm Pool. *Geophys. Res. Lett.* **39**, L01701 (2012).
13. S. M. White, A. C. Ravelo, P. J. Polissar, Dampened el niño in the early and mid-holocene due to insolation-forced warming/deepening of the thermocline. *Geophys. Res. Lett.* **45**, 316–326 (2018).
14. H. L. Ford, A. C. Ravelo, P. J. Polissar, Reduced el niño–southern oscillation during the last glacial maximum. *Science* **347**, 255–258 (2015).
15. S. A. Carolin, K. M. Cobb, J. F. Adkins, B. Clark, J. L. Conroy, S. Lejau, J. Malang, A. A. Tuen, Varied response of western Pacific hydrology to climate forcings over the Last Glacial period. *Science* **340**, 1564–1566 (2013).
16. S. Chen, S. S. Hoffman, D. C. Lund, K. M. Cobb, J. Emile-Geay, J. F. Adkins, A high-resolution speleothem record of western equatorial Pacific rainfall: Implications for Holocene ENSO evolution. *Earth Planet. Sci. Lett.* **442**, 61–71 (2016).
17. C. M. Moy, G. O. Seltzer, D. T. Rodbell, D. M. Anderson, Variability of el niño/southern oscillation activity at millennial timescales during the holocene epoch. *Nature* **420**, 162–165 (2002).
18. J. L. Conroy, J. T. Overpeck, J. E. Cole, T. M. Shanahan, M. Steinitz-Kannan, Holocene changes in eastern tropical Pacific climate inferred from a Galápagos lake sediment record. *Quat. Sci. Rev.* **27**, 1166–1180 (2008).
19. X. Wang, Z. Jian, A. Lückge, Y. Wang, H. Dang, M. Mohtadi, Precession-paced thermocline water temperature changes in response to upwelling conditions off southern Sumatra over the past 300,000 years. *Quat. Sci. Rev.* **192**, 123–134 (2018).
20. H. Dang, Z. Jian, J. Wu, F. Bassinot, T. Wang, C. Kissel, The calcification depth and Mg/Ca thermometry of *Pulleniatina obliquiloculata* in the tropical Indo-Pacific: A core-top study. *Mar. Micropaleontol.* **145**, 28–40 (2018).
21. M. Hollstein, M. Mohtadi, Y. Rosenthal, P. M. Sanchez, D. Oppo, G. M. Méndez, S. Steinke, D. Hebbeln, Stable oxygen isotopes and Mg/Ca in planktic foraminifera from modern surface sediments of the Western Pacific Warm Pool: implications for thermocline reconstructions. *Paleoceanography* **32**, (2017).
22. C. Waelbroeck, L. Labeyrie, E. Michel, J.-C. Duplessy, J. F. McManus, K. Lambeck, E. Balbon, M. Labracherie, Sea-level and deep water temperature changes derived from benthic foraminifera isotopic records. *Quat. Sci. Rev.* **21**, 295–305 (2002).
23. B. K. Linsley, Y. Rosenthal, D. W. Oppo, Holocene evolution of the Indonesian throughflow and the western Pacific warm pool. *Nat. Geosci.* **3**, 578–583 (2010).
24. D. W. Lea, D. K. Pak, H. J. Spero, Climate impact of late quaternary equatorial pacific sea surface temperature variations. *Science* **289**, 1719–1724 (2000).
25. J. F. Schröder, W. Kuhnt, A. Holbourn, S. Beil, P. Zhang, M. Hendrizan, J. Xu, Deglacial warming and hydroclimate variability in the central Indonesian Archipelago. *Paleoceanogr. Paleoclimatol.* **33**, 974–993 (2018).
26. S. A. Marcott, T. K. Bauska, C. Buizert, E. J. Steig, J. L. Rosen, K. M. Cuffey, T. J. Fudge, J. P. Severinghaus, J. Ahn, M. L. Kalk, J. R. McConnell, T. Sowers, K. C. Taylor, J. W. C. White, E. J. Brook, Centennial-scale changes in the global carbon cycle during the last deglaciation. *Nature* **514**, 616–619 (2014).
27. M. Hollstein, M. Mohtadi, Y. Rosenthal, M. Prange, D. W. Oppo, G. M. Méndez, K. Tachikawa, P. M. Sanchez, S. Steinke, D. Hebbeln, Variations in Western Pacific Warm Pool surface and thermocline conditions over the past 110,000 years: Forcing mechanisms and implications for the glacial Walker circulation. *Quat. Sci. Rev.* **201**, 429–445 (2018).
28. Z. Jian, Y. Wang, H. Dang, D. W. Lea, Z. Liu, H. Jin, Y. Yin, Half-precessional cycle of thermocline temperature in the western equatorial Pacific and its bihemispheric dynamics. *Proc. Natl. Acad. Sci. U.S.A.* **117**, 7044–7051 (2020).
29. Z. Liu, M. Alexander, Atmospheric bridge, oceanic tunnel, and global climatic teleconnections. *Rev. Geophys.* **45**, RG2005 (2007).
30. Z. Liu, S.-I. Shin, B. Otto-Bliesner, J. E. Kutzbach, E. C. Brady, D. E. Lee, Tropical cooling at the last glacial maximum and extratropical ocean ventilation. *Geophys. Res. Lett.* **29**, 1409 (2002).
31. K. Pahnke, J. P. Sachs, Sea surface temperatures of southern midlatitudes 0–160 kyr B. P. *Paleoceanography* **21**, PA2003 (2006).
32. K. Pahnke, R. Zahn, H. Elderfield, M. Schulz, 340,000-Year centennial-scale marine record of Southern Hemisphere climatic oscillation. *Science* **301**, 948–952 (2003).
33. J. Kalansky, Y. Rosenthal, T. Herbert, S. Bova, M. Altabet, Southern Ocean contributions to the Eastern Equatorial Pacific heat content during the Holocene. *Earth Planet. Sci. Lett.* **424**, 158–167 (2015).
34. S. C. Bova, T. Herbert, Y. Rosenthal, J. Kalansky, M. Altabet, C. Chazen, A. Mojarro, J. Zech, Links between eastern equatorial Pacific stratification and atmospheric CO_2 rise during the last deglaciation. *Paleoceanography* **30**, 1407–1424 (2015).
35. D. Hu, W. Cai, A. S. Gupta, A. Ganachaud, B. Qiu, A. L. Gordon, X. Lin, Z. Chen, S. Hu, G. Wang, Q. Wang, J. Sprintall, T. Qu, Y. Kashino, F. Wang, W. S. Kessler, Pacific western boundary currents and their roles in climate. *Nature* **522**, 299–308 (2015).
36. S. G. Philander, A. V. Fedorov, Role of tropics in changing the response to Milankovich forcing some three million years ago. *Paleoceanography* **18**, 1045 (2003).
37. C. A. Shields, D. A. Bailey, G. Danabasoglu, M. Jochum, J. T. Kiehl, S. Levis, S. Park, The low-resolution CCSM4. *J. Climate* **25**, 3993–4014 (2012).
38. Y. Wang, Z. Jian, P. Zhao, K. Xu, H. Dang, Z. Liu, D. Xiao, J. Chen, Precessional forced zonal triple-pole anomalies in the tropical Pacific annual cycle. *J. Climate* **32**, 7369–7402 (2019).
39. Y. Rosenthal, B. K. Linsley, D. W. Oppo, Pacific ocean heat content during the past 10,000 years. *Science* **342**, (2013).
40. P. N. DiNezio, A. Timmermann, J. E. Tierney, F.-F. Jin, B. Otto-Bliesner, N. Rosenbloom, B. Mapes, R. Neale, R. F. Ivanovic, A. Montenegro, The climate response of the Indo-Pacific warm pool to glacial sea level. *Paleoceanography* **31**, 866–894 (2016).
41. A. C. Clement, R. Seager, M. A. Cane, Orbital controls on the El Niño/Southern Oscillation and the tropical climate. *Paleoceanography* **14**, 441–456 (1999).
42. A. Koutavas, S. Joanides, El Niño–Southern Oscillation extrema in the Holocene and Last Glacial Maximum. *Paleoceanography* **27**, PA4208 (2012).
43. R. Xie, F.-F. Jin, Two leading ENSO modes and El Niño types in the Zebiak-Cane model. *J. Climate* **31**, 1943–1962 (2018).
44. M. Carré, J. P. Sachs, S. Purca, A. J. Schauer, P. Braconnot, R. A. Falcón, M. Julien, D. Lavallée, Holocene history of ENSO variance and asymmetry in the eastern tropical Pacific. *Science* **345**, 1252220 (2014).
45. A. V. Fedorov, S. G. Philander, Is El Nino Changing? *Science* **288**, 1997–2002 (2000).
46. S. A. Marcott, J. D. Shakun, P. U. Clark, A. C. Mix, A reconstruction of regional and global temperature for the past 11,300 years. *Science* **339**, 1198–1201 (2013).
47. J. Laskar, P. Robutel, F. Joutel, M. Gastineau, A. C. M. Correia, B. Levrard, A long-term numerical solution for the insolation quantities of the Earth. *Astron. Astrophys.* **428**, 261–285 (2004).

48. J. D. Shakun, P. U. Clark, F. He, S. A. Marcott, A. C. Mix, Z. Liu, B. Ottoa-Bliesner, A. Schmittner, E. Bard, Global warming preceded by increasing carbon dioxide concentrations during the last deglaciation. *Nature* **484**, 49–54 (2012).
49. L. E. Lisiecki, M. E. Raymo, A Pliocene-Pleistocene stack of 57 globally distributed benthic $\delta^{18}O$ records. *Paleoceanography* **20**, PA1003 (2005).
50. J. Yu, R. F. Anderson, Z. Jin, J. W. B. Rae, B. N. Opdyke, S. M. Eggins, Responses of the deep ocean carbonate system to carbon reorganization during the Last Glacial-interglacial cycle. *Quat. Sci. Rev.* **76**, 39–52 (2013).
51. W. Fan, Z. Jian, Z. Chu, H. Dang, Y. Wang, F. Bassinot, X. Han, Y. Bian, Variability of the Indonesian Throughflow in the Makassar Strait over the Last 30 ka. *Sci. Rep.* **8**, 5678 (2018).
52. P. Anand, H. Elderfield, M. H. Conte, Calibration of Mg/Ca thermometry in planktonic foraminifera from a sediment trap time series. *Paleoceanography* **18**, 1050 (2003).
53. Y. Rosenthal, S. Perron-Cashman, C. H. Lear, E. Bard, S. Barker, K. Billups, M. Bryan, M. L. Delaney, P. B. DeMenocal, G. S. Dwyer, H. Elderfield, C. R. German, M. Greaves, D. W. Lea, T. M. Marchitto Jr., D. K. Pak, G. L. Paradis, A. D. Russell, R. R. Schneider, K. Scheiderich, L. Stott, K. Tachikawa, E. Tappa, R. Thunell, M. Wara, S. Weldeab, P. A. Wilson, Interlaboratory comparison study of Mg/Ca and Sr/Ca measurements in planktonic foraminifera for paleoceanographic research. *Geochem. Geophys. Geosyst.* **5**, Q04D09 (2004).
54. P. A. Martin, D. W. Lea, A simple evaluation of cleaning procedures on fossil benthic foraminiferal Mg/Ca. *Geochem. Geophys. Geosyst.* **3**, 8401 (2002).
55. S. Barker, M. Greaves, H. Elderfield, A study of cleaning procedures used for foraminiferal Mg/Ca paleothermometry. *Geochem. Geophys. Geosyst.* **4**, 8407 (2003).
56. J. F. Schröder, A. Holbourn, W. Kuhnt, K. Küssner, Variations in sea surface hydrology in the southern Makassar Strait over the past 26 kyr. *Quat. Sci. Rev.* **154**, 143–156 (2016).
57. A. Y. Sadekov, R. Ganeshram, L. Pichevin, R. Berdin, E. McClymont, H. Elderfield, A. W. Tudhope, Palaeoclimate reconstructions reveal a strong link between El Niño-Southern Oscillation and Tropical Pacific mean state. *Nat. Commun.* **4**, 2692 (2013).
58. L. D. Pena, I. Cacho, P. Ferretti, M. A. Hall, El Niño–Southern Oscillation–like variability during glacial terminations and interlatitudinal teleconnections. *Paleoceanography* **23**, PA3101 (2008).
59. M. Yamamoto, R. Suemune, T. Oba, Equatorward shift of the subarctic boundary in the northwestern Pacific during the last deglaciation. *Geophys. Res. Lett.* **32**, L05609 (2005).
60. B. E. Bemis, H. J. Spero, J. Bijma, D. W. Lea, Reevaluation of the oxygen isotopic composition of planktonic foraminifera: Experimental results and revised paleotemperature equations. *Paleoceanography* **13**, 150–160 (1998).
61. J. Jouzel, V. Masson-Delmotte, O. Cattani, G. Dreyfus, S. Falourd, G. Hoffmann, B. Minster, J. Nouet, J.-M. Barnola, J. Chappellaz, H. Fischer, J. C. Gallet, S. Johnsen, M. Leuenberger, L. Loulergue, D. Luethi, H. Oerter, F. Parrenin, G. Raisbeck, D. Raynaud, A. Schilt, J. Schwander, E. Selmo, R. Souchez, R. Spahni, B. Stauffer, J. P. Steffensen, B. Stenni, T. F. Stocker, J. L. Tison, M. Werner, E. W. Wolff, Orbital and millennial antarctic climate variability over the past 800,000 years. *Science* **317**, 793–796 (2007).
62. E. J. Steig, E. J. Brook, J. W. C. White, C. M. Sucher, M. L. Bender, S. J. Lehman, D. L. Morse, E. D. Waddington, G. D. Clow, Synchronous climate changes in antarctica and the north atlantic. *Science* **282**, 92–95 (1998).
63. A. E. Shevenell, A. E. Ingalls, E. W. Domack, C. Kelly, Holocene Southern Ocean surface temperature variability west of the Antarctic Peninsula. *Nature* **470**, 250–254 (2011).
64. Y. J. Wang, H. Cheng, R. L. Edward, Z. S. An, J. Y. Wu, C.-C. Shen, J. A. Dorale, A high-resolution absolute-dated late pleistocene monsoon record from Hulu Cave, China. *Science* **294**, 2345–2348 (2001).
65. C. A. Dykoski, R. L. Edwards, H. Cheng, D. Yuan, Y. Cai, M. Zhang, Y. Lin, J. Qing, Z. An, J. Revenaugh, A high-resolution, absolute-dated Holocene and deglacial Asian monsoon record from Dongge Cave, China. *Earth Planet. Sci. Lett.* **233**, 71–86 (2005).
66. J. W. Partin, K. M. Cobb, J. F. Adkins, B. Clark, D. P. Fernandez, Millennial-scale trends in west Pacific warm pool hydrology since the Last Glacial Maximum. *Nature* **449**, 452–455 (2007).
67. A. Timmermann, S. J. Lorenz, S.-I. An, A. Clement, S.-P. Xie, The effect of orbital forcing on the mean climate and variability of the tropical Pacific. *J. Clim.* **20**, 4147–4159 (2007).
68. W. Fan, Z. Jian, F. Bassinot, Z. Chu, Holocene centennial-scale changes of the Indonesian and South China Sea throughflows: Evidences from the Makassar Strait. *Global Planet. Change* **111**, 111–117 (2013).
69. H. Dang, Z. Jian, C. Kissel, F. Bassinot, Precessional changes in the western equatorial Pacific hydroclimate: A 240 kyr marine record from the Halmahera Sea, East Indonesia. *Geochem. Geophys. Geosyst.* **16**, 148–164 (2015).
70. A. Holbourn, W. Kuhnt, J. Xu, Indonesian Throughflow variability during the last 140 ka: The Timor Sea outflow. *Geol. Soc. Spec. Publ.* **355**, 283–303 (2011).
71. H. Dang, J. Wu, Z. Xiong, P. Qiao, T. Li, Z. Jian, Orbital and sea-level changes regulate the iron-associated sediment supplies from Papua New Guinea to the equatorial Pacific. *Quat. Sci. Rev.* **239**, 106361 (2020).
72. Y. Rosenthal, D. W. Oppo, B. K. Linsley, The amplitude and phasing of climate change during the last deglaciation in the Sulu Sea, western equatorial Pacific. *Geophys. Res. Lett.* **30**, 1428 (2003).
73. L. Stott, A. Timmermann, R. Thunell, Southern Hemisphere and deep-sea warming led deglacial atmospheric CO_2 rise and tropical warming. *Science* **318**, 435–438 (2007).
74. K. Visser, R. Thunell, L. Stott, Magnitude and timing of temperature change in the Indo-Pacific warm pool during deglaciation. *Nature* **421**, 152–155 (2003).
75. C. Levi, L. Labeyrie, F. Bassinot, F. Guichard, E. Cortijo, C. Waelbroeck, N. Caillon, J. Duprat, T. de Garidel-Thoron, H. Elderfield, Low-latitude hydrological cycle and rapid climate changes during the last deglaciation. *Geochem. Geophys. Geosyst.* **8**, Q05N12 (2007).
76. F. T. Gibbons, D. W. Oppo, M. Mohtadi, Y. Rosenthal, J. Cheng, Z. Liu, B. K. Linsley, Deglacial $\delta^{18}O$ and hydrologic variability in the tropical Pacific and Indian Oceans. *Earth Planet. Sci. Lett.* **387**, 240–251 (2014).
77. M. Hendrizan, W. Kuhnt, A. Holbourn, Variability of Indonesian Throughflow and Borneo runoff during the last 14 kyr. *Paleoceanography* **32**, 1054–1069 (2017).
78. R. Y. Setiawan, M. Mohtadi, J. Southon, J. Groeneveld, S. Steinke, D. Hebbeln, The consequences of opening the Sunda Strait on the hydrography of the eastern tropical Indian Ocean. *Paleoceanography* **30**, 1358–1372 (2015).
79. M. Mohtadi, A. Lückge, S. Steinke, J. Groeneveld, D. Hebbeln, N. Westphal, Late Pleistocene surface and thermocline conditions of the eastern tropical Indian Ocean. *Quat. Sci. Rev.* **29**, 887–896 (2010).
80. M. Mohtadi, M. Prange, D. W. Oppo, R. De Pol-Holz, U. Merkel, X. Zhang, S. Steinke, A. Lückge, North Atlantic forcing of tropical Indian Ocean climate. *Nature* **509**, 76–80 (2014).

Acknowledgments: We appreciate the sea-board assistance of cruises MD122, MD181, SO185, and KX08-973 and the laboratory assistance by P. Qiao, W. Fan, and Z. Chu. **Funding:** This study is supported by the National Natural Science Foundation of China (grants 91958208, 41976047, 91428310, 41630965, and 91858106), the National Key Research and Development Program of China (grant 2018YFE0202401), and the Ministry of Natural Resources of China (grant GASI-GEOGE-04). Financial supports by the BMBF [grants 03G0806A (CARIMA) and 03G0864F (CAHOL) to M.M. and grants 03G0185A (VITAL) and 03G0217A (MAJA) to W.K.] are acknowledged. This study is implemented under the France-China Framework of LIA-MONOCL. **Author contributions:** H.D. wrote the draft of the paper, and all authors contributed to subsequent revisions. Z.J. designed the framework, and H.D. proposed the preliminary idea of this research. Z.J. took lead in the experiments, assisted by H.D. and L.Y. Y.W. carried out the numerical simulation. M.M. and Y.R. helped the interpretations. F.B. and W.K. provided part of the sediment materials and helped the accelerator mass spectrometry ^{14}C measurements. **Competing interests:** The authors declare that they have no competing interests. **Data and materials availability:** All data needed to evaluate the conclusions in the paper are present in the paper and/or the Supplementary Materials. Additional data related to this paper may be requested from the authors. All the data can also be obtained from NOAA (ncdc.noaa.gov) and PANGAEA (pangaea.de) or from Z.J. (email: jian@tongji.edu.cn).

Submitted 2 April 2020
Accepted 25 August 2020
Published 14 October 2020
10.1126/sciadv.abc0402

Citation: H. Dang, Z. Jian, Y. Wang, M. Mohtadi, Y. Rosenthal, L. Ye, F. Bassinot, W. Kuhnt, Pacific warm pool subsurface heat sequestration modulated Walker circulation and ENSO activity during the Holocene. *Sci. Adv.* **6**, eabc0402 (2020).

Pacific warm pool subsurface heat sequestration modulated Walker circulation and ENSO activity during the Holocene

Haowen Dang, Zhimin Jian, Yue Wang, Mahyar Mohtadi, Yair Rosenthal, Liming Ye, Franck Bassinot and Wolfgang Kuhnt

Sci Adv **6** (42), eabc0402.
DOI: 10.1126/sciadv.abc0402

Science Advances
AAAS

advances.sciencemag.org/cgi/content/full/6/42/eabc0402/DC1

Supplementary Materials for

Pacific warm pool subsurface heat sequestration modulated Walker circulation and ENSO activity during the Holocene

Haowen Dang, Zhimin Jian*, Yue Wang, Mahyar Mohtadi, Yair Rosenthal, Liming Ye, Franck Bassinot, Wolfgang Kuhnt

*Corresponding author. Email: jian@tongji.edu.cn

Published 14 October 2020, *Sci. Adv.* **6**, eabc0402 (2020)
DOI: 10.1126/sciadv.abc0402

The PDF file includes:

Other Supplementary Material for this manuscript includes the following:

(available at advances.sciencemag.org/cgi/content/full/6/42/eabc0402/DC1)

Data file S1

Introduction

This supporting information provides supplementary descriptions of the *Methods* applied in this study, as well as three tables giving the information of the sediment cores compiled in this study (*Table S1*), the Mg/Ca measurement reproductivity (*Table S2*) and radiocarbon dates of the cores firstly published in this study (*Table S3*).

Section S1: The *P. obliquiloculata* Mg/Ca records and dissolution effect

We argue that the possible dissolution effect is not a major factor influencing the variations in the IPWP *P. obliquiloculata* Mg/Ca records. Firstly, all the studied cores are retrieved from water depth above ~2800 m (Fig. S1), and the changes in bottom water carbonate ion concentration ($[CO_3^{2-}]$) are less than ±5 μmol/kg in the western tropical Pacific at 2.3 km water depth (based on benthic foraminifera B/Ca reconstruction; 50). Such a $[CO_3^{2-}]$ change may result in a variation in *P. obliquiloculata* Mg/Ca of 8.5±0.5% (about 0.24-0.27 mmol/mol, assuming mean Mg/Ca = 3 mmol/mol), given a Mg/Ca-$[CO_3^{2-}]$ sensitivity of 1.6-1.8% (20). However, the bottom water $[CO_3^{2-}]$ variations in the last 25 ka show no trend (Fig. 6c in 50) and thus may not result in the patterns of the *P. obliquiloculata* Mg/Ca records analyzed in this study.

Secondly, either the Early-Holocene peak (EH-peak) or the Middle-Holocene peak (MH-peak) types of *P. obliquiloculata* Mg/Ca records occurs in all the studied cores from a water depth range of 730-2299 m and 1094-2816 m for the EH-peak and MH-peak types, respectively (Fig. S1). Both the amplitudes of (1) LGM to the Early-Holocene and (2) through the Holocene are identical of ~1 mmol/mol for all the records of EH-peak type (Fig. S1, left panel). For the MH-peak type, the Mg/Ca increases from ~15 ka to ~10 ka are similarly ~1 mmol/mol, and the decreases from Middle to Late Holocene are around 0.5 mmol/mol (Fig. S1, right panel). If there were a bottom water dissolution effect, it would not explain the similarities of these Mg/Ca changes, especially their similar amplitudes, over the intermediate and deeper water depths.

Finally, the benthic B/Ca records from 3.4-4.3 km water depth of equatorial Pacific show a decrease in $[CO_3^{2-}]$ of ~8-15 μmol/kg from the Early to Late Holocene (50), and may explain ~12-22% decrease in *P. obliquiloculata* Mg/Ca (20). From LGM to the Early Holocene, the deep Pacific $[CO_3^{2-}]$ increased by ~14-25 μmol/kg (50) and may result in an increase of 15~27% of *P. obliquiloculata* Mg/Ca (20). So, if bottom water $[CO_3^{2-}]$ of shallower depth of IPWP did change in a similar manner and amplitude as those seen in the open equatorial Pacific, the possible changes in *P. obliquiloculata* Mg/Ca due to dissolution effect would be less than 30%.

Section S2: Reconstructions of proxy data

2.1 Correction for the possible bias effects on Mg/Ca

The planktonic foraminifera Mg/Ca derived temperatures may differ significantly due to the differences in calibration equations (20, 21) and/or the different pre-treatment procedures (especially the cleaning method, 10, 51). We calculated the anomalies (SSTA and TWTA) of the calibrated temperature (SST and TWT) relative to a certain baseline, to minimize or reduce these possible biases. Here we take the average values over 6-10 ka of each record as the baseline, i.e., we subtracted the 6-10 ka average from each data point to obtain its anomaly.

Taking the records of MD10-3340 for an example (Fig. S2), the SST results calculated by calibrations developed from the equatorial Pacific (24), the Sargasso Sea sediment trap (52) and tropical Pacific core-tops (21) show differences as large as ~5°C (Fig. S2A). But the SSTAs differ less than 0.1°C among these calibrations (Fig. S2B). Similarly, TWT given by calibrations of Ref. 20, 21, 52 differs by 0.8-4°C (Fig. S2C), but the differences in TWTA are much smaller as 0.05°C (Fig. S2D).

Except the possible bias of Mg/Ca-temperature calculated by different calibrations, the Mg/Ca ratio produced in different laboratory (53) and by different cleaning method (21) may also introduce biases in the reconstructed temperature results. Studies in the Indonesian seas (10, 51) detected a decrease as large as 6% in the measured Mg/Ca of both *G. ruber* and *P. obliquiloculata* following a reductive cleaning (54) compared to the non-reductive cleaning (55). We calculated such a possible effect on the Mg/Ca of *G. ruber* and *P. obliquiloculata* of MD10-3340, by randomly increasing the Mg/Ca value by 6±1.5% (uniformly distributing between 4.5% and 7.5%) and then calculating the SST and TWT, respectively (using equations of Ref. 21). The SST (Fig. S2E) and TWT (Fig. S2G) of increased Mg/Ca are higher than the original ones by 0.6°C on average, but the

SSTA (Fig. S2F) and TWTA (Fig. S2H) show almost no difference between the two sets of Mg/Ca (~0.01°C on average).

These assessments suggest that the possible biases induced by either calibrations or measurements are significantly reduced when the calculations of anomalies are applied. This is essentially because the Mg/Ca-temperature sensitivity is rather identical for most planktonic foraminifera species. Therefore, rather than a loose constraint on the absolute temperature estimates due to those possible biases, a more reliable measure of the relative changes may be acquired across the records by calculating the temperature anomalies.

2.2 Dating uncertainties

Dating of co-existed wood fragments and planktonic foraminifera in a sediment core from the Makassar Strait shows variations of the ^{14}C reservoir age ranging between 100 and 1100 yr (56) over the LGM-Holocene. Applying a variable reservoir age may introduce differences in the calibrated calendar ages at an order of several hundred years. We did not apply such a variable reservoir age method in all the cores of this study, because the spatial and temporal coverages of such ^{14}C reservoir age variations is not fully explored yet. In other words, it would be difficult to determine the reservoir age variations outside the Makassar Strait. Also, differences of calendar age induced by variations of reservoir age (10^2 yr) is much smaller than the time-scale of the main issues considered in this study (10^3-10^4 yr). Therefore, ages determined by constant or variable reservoir ages are both acceptable for this study, but one should keep in mind about the possible error range (several hundred years) of the age model.

2.3 Zonal and meridional temperature anomaly gradients

In addition to the equatorial Pacific west-east zonal SST gradient published before (42), we calculated the W-E zonal subsurface temperature gradient in this study. The eastern equatorial Pacific (EEP) subsurface temperatures were reconstructed by Mg/Ca of *Neogloboquadrina dutertrei* from three sediment cores (Supplementary Table S1). The habitat depth of *N. dutertrei* is predicted to be slightly deeper than *P. obliquiloculata* (21) and thus in the deeper thermocline in EEP (33, 57, 58). The difference between the *P. obliquiloculata* Mg/Ca derived TWT of IPWP and the *N. dutertrei* Mg/Ca derived deep thermocline temperature (DTT) of EEP may be interpreted as the subsurface temperature gradient across the W-E equatorial Pacific. We calculated the EEP DTT anomalies and performed the binning averages for the three records using the same method at a 150 yr step as for IPWP TWTA. The sub-TA gradient (Δsub-TA) was then generated by calculating the difference between the mean IPWP TWTA (of all 11 records) and the mean EEP DTTA (of all 3 records).

Core MD97-2120 (45.5°S, 174.9°E, water depth 1210 m; 31, 32) from the southern Chatam Rise, Southwestern Pacific, and core MD01-2421 (36.0°N, 141.8°E, water depth 2224 m; 59) locate at the western margins of the south and north Pacific Sub-tropical Gyres, respectively. The SST records from these two cores represent the changes in sub-tropical western Pacific sea surface conditions. We did binning average at a 1000 yr step on the SST records from these two cores, as their original records yield time-resolutions up to ~500 yr. Then the SSTAs are calculated in the same manner as for IPWP SSTA, taking the average of 6-10 ka as the baseline. The mean IPWP SSTA is also re-calculated at a 1000 yr step. Finally, the differences between mean IPWP SSTA and the sub-tropical SSTA records are calculated to represent the meridional SSTA gradients.

2.4 *G. ruber* $\delta^{18}O$ and seawater $\delta^{18}O$

The *G. ruber* $\delta^{18}O$ records of 22 cores (Table S1) are calculated for the $\delta^{18}O_G$ anomaly ($\delta^{18}O_G$-A, PDB ‰) relative to their respective average over 6-10 ka, and then binning averaged with a 150-

yr window. The average of all records at each 150-yr window are reported as the mean $\delta^{18}O_G$-A of the IPWP, and the standard error as the error range.

These 22 records are also used to estimate the surface seawater $\delta^{18}O$ ($\delta^{18}O_{sw}$, SMOW‰). Firstly, the temperature effect is subtracted from the $\delta^{18}O_G$ using the equation of SST = 16.9 - 4.38*($\delta^{18}O_G$ - $\delta^{18}O_{sw}$) + 0.1*($\delta^{18}O_G$ - $\delta^{18}O_{sw}$)^2, and a 0.27 ‰ correction of SMOW relative to PDB is added (60). Subsequently, the $\delta^{18}O_{sw}$ is corrected for ice-volume effect using the global mean sea-level change of (22). Then, the ice-volume corrected $\delta^{18}O_{sw}$ records are calculated into anomalies relative to their respective 6-10 ka average, and then binning averaged with a 150-yr window. Finally, the average of all $\delta^{18}O_{sw}$ anomaly records at each 150-yr window are reported as the mean $\delta^{18}O_{sw}$ of the IPWP, and their standard error as the error range.

Fig. S1. *P. obliquiloculata* Mg/Ca records from different water depth.
(A) the early-Holocene peak-type (EH-peak type) mean TWTA, and (B-D) records showing EH-peak type from the northern western tropical Pacific (B, MD2188 and MD3067), equatorial western Pacific (C, GeoB17419 and KX21-2) and the Timor Sea (D, MD2378, SO18460 and SO18480). (E) the middle-Holocene peak-type (MH-peak type) mean TWTA, and (F-H) records showing MH-peak type from the equatorial western Pacific (F, MD3340; G, MD2386) and the Makassar Strait (H, MD2161 and MD2178). Water depth of each core is shown in brackets.

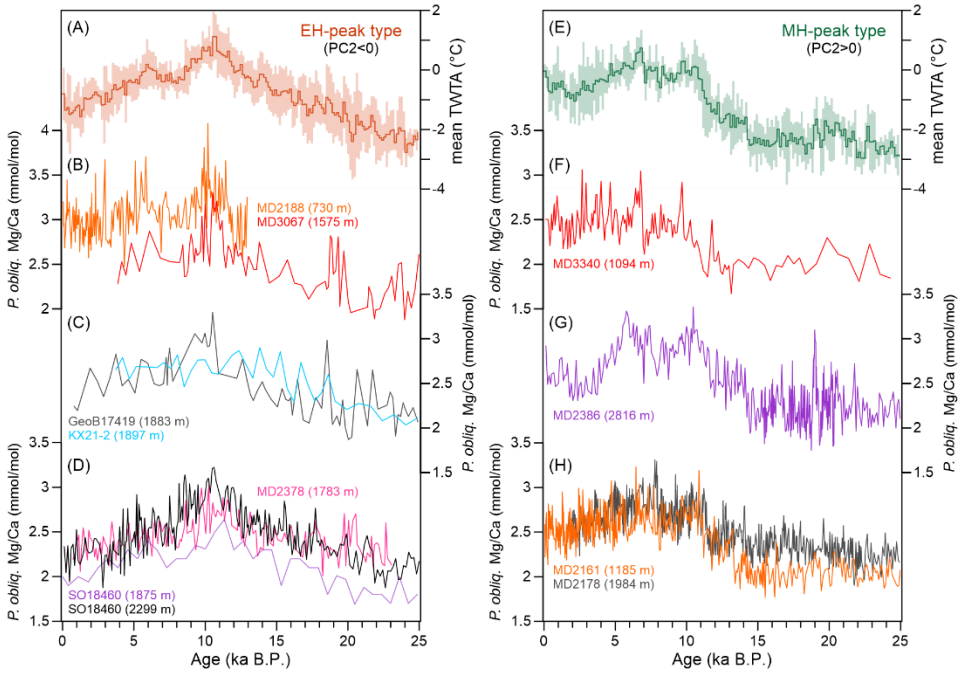

Fig. S2. Comparison of the Mg/Ca-temperature records among calibrations and cleaning-methods.

The records of MD10-3340 is taken as an example. (A-D) comparisons among calibrations for *G. ruber* Mg/Ca derived SST and SSTA (A, B) and for *P. obliquiloculata* Mg/Ca derived TWT and TWTA (C, D). (E-H) comparisons between cleaning methods for SST and SSTA (E, F) and for TWT and TWTA (G, H). Calibrations shown here are from Ref. 20, 21, 24 and 52. Differences in Mg/Ca of 6% (10, 51) are applied for the comparison between cleaning methods.

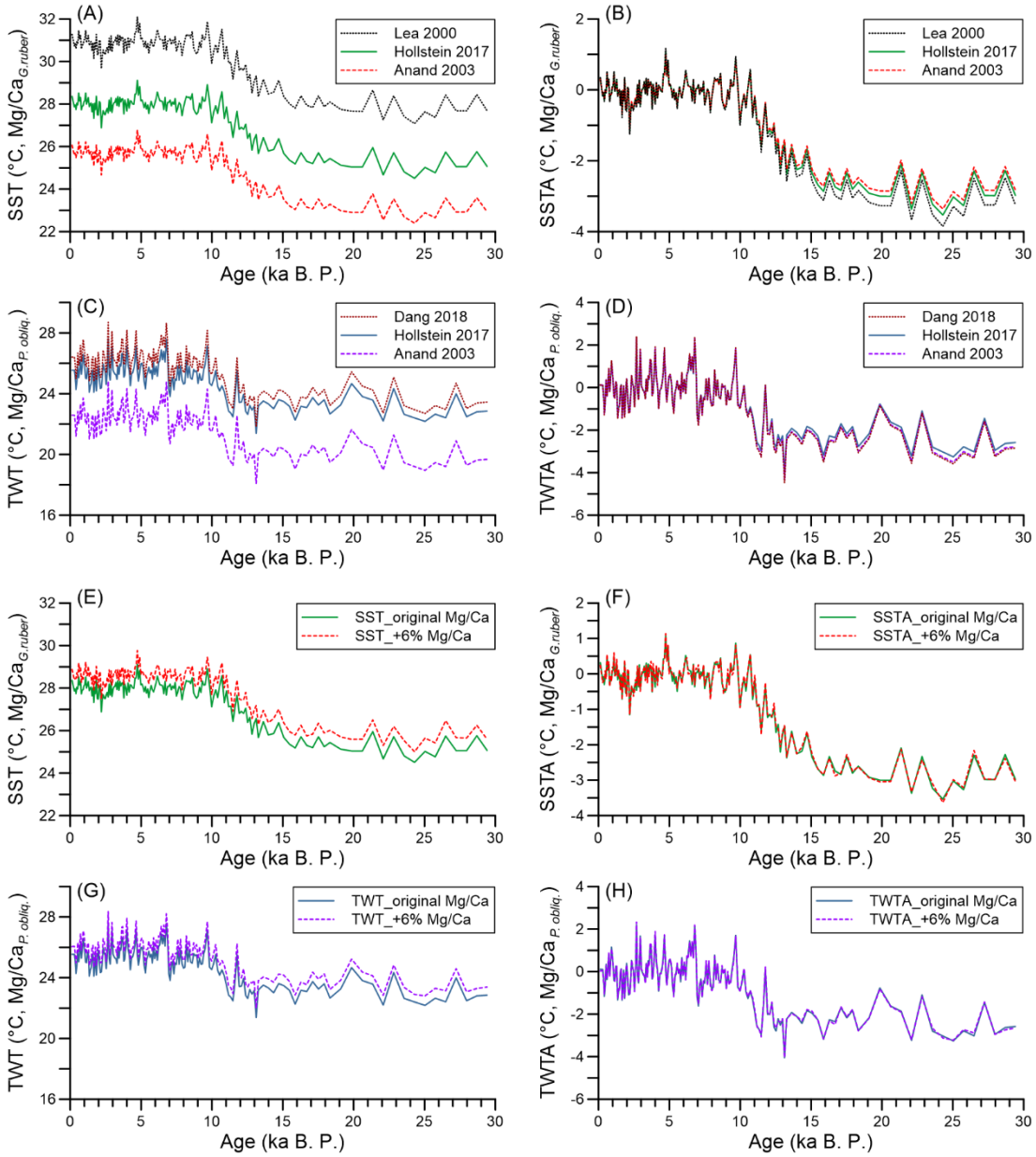

Fig. S3. Comparison of the TWTA changes with other records.

Left Panel: The Early-Holocene peak type TWTA changes. (A) the mean TWTA of Early-Holocene peak type (brown), precession (red) and obliquity (gray, 47). (B) meridional SSTA gradient between southwest Pacific (SWP, site MD97-2120) (31, 32) and IPWP. (C) Antarctic ice core δD (61, 62) and SST off West Antarctic Peninsula (ODP1098) (63). (D) speleothem $\delta^{18}O$ of the Hulu Cave (dark blue) (64) and Dongge Cave (light blue) (65).

Right Panel: The Middle-Holocene peak type TWT changes. (A) the mean TWTA of Middle-Holocene peak type (brown) and the September 21st insolation at the Equator (red) and obliquity (gray, 47). (B) U_k^{37}-SSTA of Northwest Pacific (pink) (59). (C) the zonal ΔSSTA (light green) (42) and Δsub-TA (subsurface temperature anomaly differences, calculated by the mean TWTA of IPWP and mean DTT of EEP) between the WEP and EEP. (D) $\delta^{18}O$ records of Northern Borneo stalagmites (dark green, 66; and light green, 15, 16). (E) the difference of *G. ruber* $\delta^{18}O$ between the western equatorial boundary (WEB, average of records from MD3340 and MD2386) and Ontong-Java Plateau (OJP, average of records from KX21-2 and ODP807). (F) simulated Nino3 SSTA (orange) (41) and Nino3 annual wavelet variance (black) (67). Climatic intervals of LGM, last Deglacial, Holocene and the Heinrich Stadial 1 (HS-1) and Younger Dryas (YD) events are denoted.

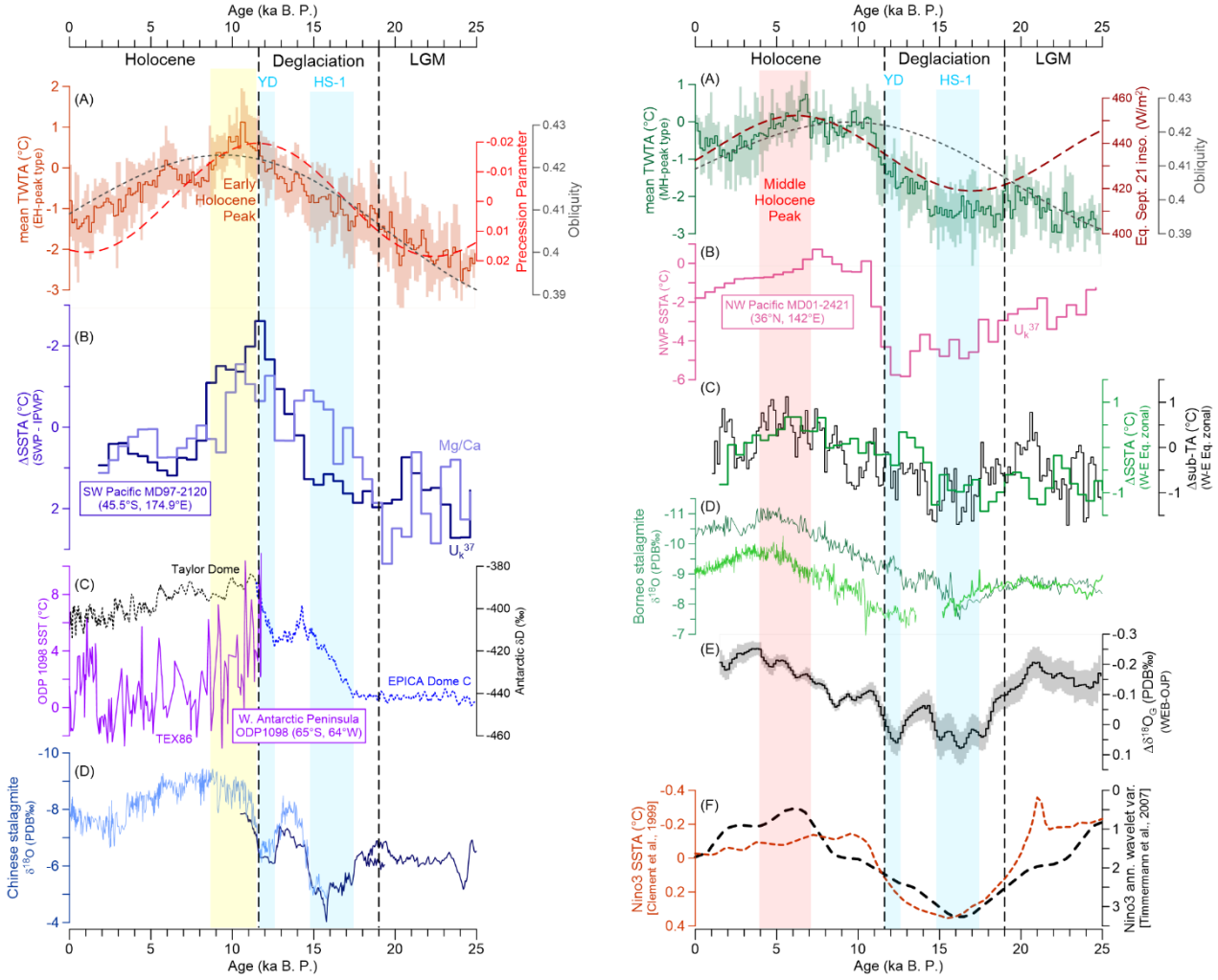

Fig. S4. CESM simulated Pacific sub-surface temperature responses to obliquity and CO_2 forcings.

(A) temperature anomaly at 120 m water depth under the forcing of obliquity (outputs of obliquity maximum minus those of obliquity minimum). An obliquity maximum would result in cooling in the subsurface waters from middle- to low-latitudes. (B, C) temperature anomalies of GHG forcing, at 120 m water depth (B) and along the equatorial Pacific profile (5°S-5°N) (C), calculated by the integrated outputs of GHG maxima minus those of GHG minima. Scale-bar for color shading is shown below. The effect of GHG increase is an overall heating of the whole Pacific with larger amplitudes in the sub-tropical gyre center and an anomalous El Nino-like subsurface temperature pattern along the equator.

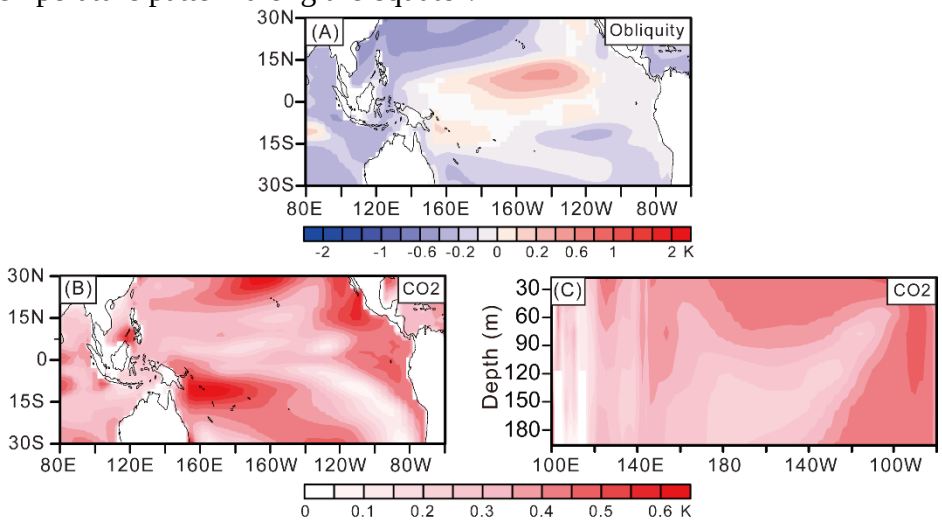

Table S1. The sediment cores analyzed in this study[#].

Site No.	Site ID	Core ID	Region	Latitude (°N)	Longitude (°E)	WD (m)	RL (ka)	MSR (cm/ka)	MSI (yr)	Reference
records of paired SST and TWT										
1	MD98-2188	MD2188	W. Philippine Sea	14.82	123.49	730	13	30	66	12
2	MD06-3067	MD3067[+]	Davo Bay	6.52	126.50	1575	30	12	265	11
3	MD98-2178	MD2178[+]	N. Makassar St.	3.62	118.70	1984	30	60	41	51, 68
4	MD01-2386	MD2386[+]	SW. Philippine Sea	1.13	129.79	2816	30	29	50	28
5	MD10-3340	MD3340[+]	Halmahera Sea	-0.52	128.72	1094	30	13	178	this study, 69
6	MD98-2161	MD2161[+]	S. Makassar St.	-5.21	117.48	1185	29	33	61	50, 68
7	SO18460	SO18460[+]	Timor Sea	-8.79	128.64	1875	30	15	670	70
8	SO18480-3	SO18480[+]	Timor Sea	-12.06	121.65	2299	30	11	160	this study
9	MD01-2378	MD2378[+]	Timor Sea	-13.08	121.79	1783	23	18	131	10
10	KX973-21-2	KX21-2[+]	Ontong-Java Plateau	-1.42	157.98	1897	30	1.5	570	this study, 71
11	GeoB17419-1	GeoB17419	E. Papua New Guinea	-2.81	144.50	1883	30	12	349	27
records of only SST										
1	MD97-2141	MD2141[+]	Sulu Sea	8.78	121.28	3633	22	23	90	72
2	MD98-2181	MD2181[+]	Davo Bay	6.45	125.83	2114	23	64	50	73
3	70GGC	70GGC	S. Makassar St.	-3.57	119.38	482	14	28	125	23
4	GIK18515-3	GIK18515[+]	S. Makassar St.	-3.63	119.36	688	30	47	80	56
5	MD98-2162	MD2162[+]	S. Makassar St.	-4.68	117.90	1855	24	45	415	74
6	13GGC	13GGC	S. Makassar St.	-7.40	115.20	594	11	49	40	23
7	MD98-2165	MD2165	Sumba St.	-9.65	118.33	2100	26	28	200	75
8	GeoB10069-3	GeoB10069[+]	Savu Sea	-9.60	120.92	1250	30	27	190	76
9	MD98-2170	MD2170[+]	Timor Sea	-10.60	125.38	832	22	25	300	72
10	MD01-2176	MD2176[+]	Seram Sea	-5.00	133.45	2382	21	50	75	72
11	GIK18517-2	GIK18517[+]	S. Makassar St.	-1.54	117.56	698	14	100	45	77
12	GIK18519-2	GIK18519[+]	C. Makassar St.	-0.57	118.11	1658	25	21	173	25
13	GIK18522-3	GIK18522[+]	N. Makassar St.	1.40	119.08	975	25	27	185	25
14	GIK18526-3	GIK18526[+]	S. Makassar St.	-3.61	118.17	1524	25	37	267	25
15	GIK18540-3	GIK18540[+]	Flores Sea	-6.87	119.58	1189	24	18	197	25
16	TGS-931*	TGS-931[+]	NW. Banda Sea	-2.41	122.62	1912	19	20	105	25
Eastern equatorial Pacific records										
1	ODP1240	ODP1240	EEP	0.02	279.54	2921	30	14	146	58
2	CD38-17P	CD38-17	EEP	-1.60	269.57	2580	23	6	376	57
3	KNR195-5 CDH-23	CDH-23	Peru Margin	-3.75	278.9	374	11	100	69	33

WD: water depth, RL: record length, MSR: mean sedimentation rate, MSI: mean sampling interval.

[#]: records from the west off Sunda Strait (78, 79) and from southwest off Sumatra (19, 80) are not included in this compilation, as they mainly reflect local processes of Sunda Strait Outflow and Sumatra Upwelling, respectively.

*: record TGS-931 covers only 10-19 ka.

+: record of *G. ruber* $\delta^{18}O$ is analyzed for the $\delta^{18}O_G$-anomaly and surface seawater $\delta^{18}O$ anomaly.

Table S2. Mg/Ca measurement reproductivity of core MD10-3340, SO18480, KX21-2 and MD01-2386.

Core	*G. ruber* Mg/Ca		*P. obliquiloculata* Mg/Ca	
	No. Rep.	RSD	No. Rep.	RSD
MD10-3340	72	2.4	60	5.4
SO18480	72	1.8	70	3.9
KX21-2	48	2.1	41	5.2
MD01-2386	119	2.5	131	4.9
Sum	**311**	**2.2**	**302**	**4.8**

Table S3. Radiocarbon dates of core MD10-3340, SO18480-3, and KX973-21-2.

MD10-3340 AMS ^{14}C dates					
Core depth (cm)	^{14}C age (yr)	Reservoir Age (yr)	Calendar age (yr)	Calendar age range or error (1s)	Lab
24	1140 ±30	348 ±46	655	±50	Beta Analytic
74	2560 ±30	348 ±46	2191.5	±78.5	Beta Analytic
138	4390 ±30	348 ±46	4472.5	±73.5	Beta Analytic
206	7020 ±30	348 ±46	7466.5	±48.5	Beta Analytic
244	8870 ±40	348 ±46	9477	±48	Beta Analytic
296	11870 ±50	348 ±46	13289.5	±70.5	Beta Analytic
324	16320 ±60	348 ±46	19111	±113	Beta Analytic
368	22980 ±90	348 ±46	26849	±186	Beta Analytic
416	30910 ±160	348 ±46	34428.5	±180.5	Beta Analytic
SO18480-3 AMS ^{14}C dates					
Core depth (cm)	^{14}C age (yr)	Reservoir Age (yr)	Calendar age (yr)	Calendar age range or error (1s)	Lab
8.5	1490 ±25	345 ±24	972	(900-1056)	Leibniz Lab, Kiel Univ.
28.5	3625 ±30	345 ±24	3449	(3354-3556)	Leibniz Lab, Kiel Univ.
50.5	4175 ±35	345 ±24	4166	(4010-4318)	Leibniz Lab, Kiel Univ.
71.5	5520 ±35	345 ±24	5830	(5715-5922)	Leibniz Lab, Kiel Univ.
94.5	7710 ±40	345 ±24	8102	(7980-8216)	Leibniz Lab, Kiel Univ.
116.5	8960 ±45	345 ±24	9551	(9452-9690)	Leibniz Lab, Kiel Univ.
139.5	11055 ±55	345 ±24	12633	(12376-12539)	Leibniz Lab, Kiel Univ.
158.5	12715 ±60	345 ±24	14112	(13907-14445)	Leibniz Lab, Kiel Univ.
183.5	14200 ±70	345 ±24	16355	(15983-16772)	Leibniz Lab, Kiel Univ.
202.5	15530 ±80	345 ±24	18360	(18063-18652)	Leibniz Lab, Kiel Univ.
224.5	18090 ±100	345 ±24	20796	(20467-21196)	Leibniz Lab, Kiel Univ.
260.5	20580 +130/-120	345 ±24	24081	(23743-24437)	Leibniz Lab, Kiel Univ.
300.5	23400 +170/-160	345 ±24	27711	±237 (1σ)	Leibniz Lab, Kiel Univ.
350.5	27600 +270/-260	345 ±24	32616	±326 (1σ)	Leibniz Lab, Kiel Univ.
390.5	30440 +360/-350	345 ±24	35527	±363 (1σ)	Leibniz Lab, Kiel Univ.
440.5	34570 +590/-550	345 ±24	39627	±598 (1σ)	Leibniz Lab, Kiel Univ.
492.5	41020 +1970/-1580	345 ±24	45309	±2043 (1σ)	Leibniz Lab, Kiel Univ.

KX973-21-2 AMS ^{14}C dates					
Core depth (cm)	^{14}C age (yr)	Reservoir Age (yr)	Calendar age (yr)	Calendar age range or error (1s)	Lab
0.5	3860 ±30	376 ±96	3791	(3648-3917)	Beta Analytic
32.5	16360 ±50	376 ±96	19219	(19050-19372)	Beta Analytic

Caption for Data Table S1.

The supplementary Data Table S1 (Excel file) includes two sets of data-sheets (six sheets).

Set 1: the mean anomaly stacks of SSTA (sheet 1), TWTA (sheet 2), and $\delta^{18}O_{sw}$ (sheet 3) of IPWP over the last 25 ka, with column A (Age, at the start point of the 150-yr bins), B (number of records with available data), C (stacked mean anomaly of the variable) and D (standard deviation of the records taken into account). For $\delta^{18}O_{sw}$ stack, the standard error of the records are calculated (Column E).

Set 2: the records of Mg/Ca and calibrated temperatures of Cores MD10-3340 (sheet 4), SO18480 (sheet 5) and KX21-2 (sheet 6) firstly reported in this study.

REFERENCES

1. D. Gu, S. G. H. Philander, Interdecadal climate fluctuations that depend on exchanges between the tropics and extratropics. *Science* **275**, 805–807 (1997).
2. A. Timmermann, S.-I. An, J.-S. Kug, F.-F. Jin, W. Cai, A. Capotondi, K. M. Cobb, M. Lengaigne, M. J. McPhaden, M. F. Stuecker, K. Stein, A. T. Wittenberg, K.-S. Yun, T. Bayr, H.-C. Chen, Y. Chikamoto, B. Dewitte, D. Dommenget, P. Grothe, E. Guilyardi, Y.-G. Ham, M. Hayashi, S. Ineson, D. Kang, S. Kim, W. M. Kim, J.-Y. Lee, T. Li, J.-J. Luo, S. M. Gregor, Y. Planton, S. Power, H. Rashid, H.-L. Ren, A. Santoso, K. Takahashi, A. Todd, G. Wang, G. Wang, R. Xie, W.-H. Yang, S.-W. Yeh, J. Yoon, E. Zeller, X. Zhang, El Niño–Southern oscillation complexity. *Nature* **559**, 535–545 (2018).
3. S. McGregor, A. Timmermann, M. F. Stuecker, M. H. England, M. Merrifield, F.-F. Jin, Y. Chilkamoto, Recent Walker circulation strengthening and Pacific cooling amplified by Atlantic warming. *Nat. Clim. Change* **4**, 888–892 (2014).
4. W. Cai, L. Wu, M. Langaigne, T. Li, S. McGregor, J.-S. Kug, J.-Y Yu, M. F. Stuecker, A. Santoso, X. Li, Y.-G. Ham, Y. Chikamoto, B. Ng, M. J. McPhaden, Y. Du, D. Dommenget, F. Jia, J. B. Kajtar, N. Keenlyside, X. Lin, J.-J. Luo, M. Martín-Rey, Y. Ruprich-Robert, G. Wang, S.-P. Xie, Y. Yang, S. M. Kang, J.-Y. Choi, B. Gan, G.-I. Kim, C.-E. Kim, S. Kim, J.-H. Kim, P. Chang, Pantropical climate interactions. *Science* **363**, eaav4236 (2019).
5. M. H. England, S. McGregor, P. Spence, G. A. Meehl, A. Timmermann, W. Cai, A. S. Gupta, M. J. McPhaden A. Purich, A. Santoso, Recent intensification of wind-driven circulation in the Pacific and the ongoing warming hiatus. *Nat. Clim. Change* **4**, 222–227 (2014).
6. Z. Liu, Z. Jian, C. J. Poulsen, L. Zhao, Isotopic evidence for twentieth-century weakening of the Pacific Walker circulation. *Earth Planet. Sci. Lett.* **507**, 85–93 (2019).
7. W. Cai, G. Wang, B. Dewitte, L. Wu, A. Santoso, K. Takahashi, Y. Yang, A. Carréric, M. J. McPhaden, Increased variability of eastern pacific El Niño under greenhouse warming. *Nature* **564**, 201–206 (2018).
8. N. Ramesh, R. Murtugudde, All flavours of El Niño have similar early subsurface origins. *Nat. Clim. Change* **3**, 42–46 (2013).
9. R. Neale, J. Slingo, The Maritime Continent and its role in the global climate: A GCM study. *J. Climate* **16**, 834–848 (2003).
10. J. Xu, A. Holbourn, W. Kuhnt, Z. Jian, H. Kawamura, Changes in the thermocline structure of the Indonesian outflow during Terminations I and II. *Earth Planet. Sci. Lett.* **273**, 152–162 (2008).
11. T. Bolliet, A. Holbourn, W. Kuhnt, C. Laj, C. Kissel, L. Beaufort, M. Kienast, N. Andersen, D. Garbe-Schrönberg, Mindanao Dome variability over the last 160 kyr: Episodic glacial cooling of the West Pacific Warm Pool. *Paleoceanography* **26**, PA1208 (2011).

12. H. Dang, Z. Jian, F. Bassinot, P. Qiao, X. Cheng, Decoupled Holocene variability in surface and thermocline water temperatures of the Indo-Pacific Warm Pool. *Geophys. Res. Lett.* **39**, L01701 (2012).
13. S. M. White, A. C. Ravelo, P.J. Polissar, Dampened el niño in the early and mid-holocene due to insolation-forced warming/deepening of the thermocline. *Geophys. Res. Lett.* **45**, 316–326 (2018).
14. H. L. Ford, A. C. Ravelo, P. J. Polissar, Reduced el niño–southern oscillation during the last glacial maximum. *Science* **347**, 255–258 (2015).
15. S. A. Carolin, K. M. Cobb, J. F. Adkins, B. Clark, J. L. Conroy, S. Lejau, J. Malang, A. A. Tuen, Varied response of western Pacific hydrology to climate forcings over the Last Glacial period. *Science* **340**, 1564–1566 (2013).
16. S. Chen, S. S. Hoffman, D. C. Lund, K. M. Cobb, J. Emile-Geay, J. F. Adkins, A high-resolution speleothem record of western equatorial Pacific rainfall: Implications for Holocene ENSO evolution. *Earth Planet. Sci. Lett.* **442**, 61–71 (2016).
17. C. M. Moy, G. O. Seltzer, D. T. Rodbell, D. M. Anderson, Variability of el niño/southern oscillation activity at millennial timescales during the holocene epoch. *Nature* **420**, 162–165 (2002).
18. J. L. Conroy, J. T. Overpeck, J. E. Cole, T. M. Shanahan, M. Steinitz-Kannan, Holocene changes in eastern tropical Pacific climate inferred from a Galápagos lake sediment record. *Quat. Sci. Rev.* **27**, 1166–1180 (2008).
19. X. Wang, Z. Jian, A. Lückge, Y. Wang, H. Dang, M. Mohtadi, Precession-paced thermocline water temperature changes in response to upwelling conditions off southern Sumatra over the past 300,000 years. *Quat. Sci. Rev.* **192**, 123–134 (2018).
20. H. Dang, Z. Jian, J. Wu, F. Bassinot, T. Wang, C. Kissel, The calcification depth and Mg/Ca thermometry of *Pulleniatina obliquiloculata* in the tropical Indo-Pacific: A core-top study. *Mar. Micropaleontol.* **145**, 28–40 (2018).
21. M. Hollstein, M. Mohtadi, Y. Rosenthal, P. M. Sanchez, D. Oppo, G. M. Méndez, S. Steinke, D. Hebbeln, Stable oxygen isotopes and Mg/Ca in planktic foraminifera from modern surface sediments of the Western Pacific Warm Pool: implications for thermocline reconstructions. *Paleoceanography* **32**, (2017).
22. C. Waelbroeck, L. Labeyrie, E. Michel, J.-C. Duplessy, J. F. McManus, K. Lambeck, E. Balbon, M. Labracherie, Sea-level and deep water temperature changes derived from benthic foraminifera isotopic records. *Quat. Sci. Rev.* **21**, 295–305 (2002).
23. B. K. Linsley, Y. Rosenthal, D. W. Oppo, Holocene evolution of the Indonesian throughflow and the western Pacific warm pool. *Nat. Geosci.* **3**, 578–583 (2010).
24. D. W. Lea, D. K. Pak, H. J. Spero, Climate impact of late quaternary equatorial pacific sea surface temperature variations. *Science* **289**, 1719–1724 (2000).
25. J. F. Schröder, W. Kuhnt, A. Holbourn, S. Beil, P. Zhang, M. Hendrizan, J. Xu, Deglacial warming and hydroclimate variability in the central Indonesian Archipelago. *Paleoceanogr. Paleoclimatol.* **33**, 974–993 (2018).

26. S. A. Marcott, T. K. Bauska, C. Buizert, E. J. Steig, J. L. Rosen, K. M. Cuffey, T. J. Fudge, J. P. Severinghaus, J. Ahn, M. L. Kalk, J. R. McConnell, T. Sowers, K. C. Taylor, J. W. C. White, E. J. Brook, Centennial-scale changes in the global carbon cycle during the last deglaciation. *Nature* **514**, 616–619 (2014).
27. M. Hollstein, M. Mohtadi, Y. Rosenthal, M. Prange, D. W. Oppo, G. M. Méndez, K. Tachikawa, P. M. Sanchez, S. Steinke, D. Hebbeln, Variations in Western Pacific Warm Pool surface and thermocline conditions over the past 110,000 years: Forcing mechanisms and implications for the glacial Walker circulation. *Quat. Sci. Rev.* **201**, 429–445 (2018).
28. Z. Jian, Y. Wang, H. Dang, D. W. Lea, Z. Liu, H. Jin, Y. Yin, Half-precessional cycle of thermocline temperature in the western equatorial Pacific and its bihemispheric dynamics. *Proc. Natl. Acad. Sci. U.S.A.*, **117**, 7044–7051 (2020).
29. Z. Liu, M. Alexander, Atmospheric bridge, oceanic tunnel, and global climatic teleconnections. *Rev. Geophys.* **45**, RG2005 (2007).
30. Z. Liu, S.-I. Shin, B. Otto-Bliesner, J. E. Kutzbach, E. C. Brady, D. E. Lee, Tropical cooling at the last glacial maximum and extratropical ocean ventilation. *Geophys. Res. Lett.* **29**, 1409 (2002).
31. K. Pahnke, J. P. Sachs, Sea surface temperatures of southern midlatitudes 0–160 kyr B. P. *Paleoceanography* **21**, PA2003 (2006).
32. K. Pahnke, R. Zahn, H. Elderfield, M. Schulz, 340,000-Year centennial-scale marine record of Southern Hemisphere climatic oscillation. *Science* **301**, 948–952 (2003).
33. J. Kalansky, Y. Rosenthal, T. Herbert, S. Bova, M. Altabet, Southern Ocean contributions to the Eastern Equatorial Pacific heat content during the Holocene. *Earth Planet. Sci. Lett.* **424**, 158–167 (2015).
34. S. C. Bova, T. Herbert, Y. Rosenthal, J. Kalansky, M. Altabet, C. Chazen, A. Mojarro, J. Zech, Links between eastern equatorial Pacific stratification and atmospheric CO_2 rise during the last deglaciation. *Paleoceanography* **30**, 1407–1424 (2015).
35. D. Hu, W. Cai, A. S. Gupta, A. Ganachaud, B. Qiu, A. L. Gordon, X. Lin, Z. Chen, S. Hu, G. Wang, Q. Wang, J. Sprintall, T. Qu, Y. Kashino, F. Wang, W. S. Kessler, Pacific western boundary currents and their roles in climate. *Nature* **522**, 299–308 (2015).
36. S. G. Philander, A. V. Fedorov, Role of tropics in changing the response to Milankovich forcing some three million years ago. *Paleoceanography* **18**, 1045 (2003).
37. C. A. Shields, D. A. Bailey, G. Danabasoglu, M. Jochum, J. T. Kiehl, S. Levis, S. Park, The low-resolution CCSM4. *J. Climate* **25**, 3993–4014 (2012).
38. Y. Wang, Z. Jian, P. Zhao, K. Xu, H. Dang, Z. Liu, D. Xiao, J. Chen, Precessional forced zonal triple-pole anomalies in the tropical Pacific annual cycle. *J. Climate* **32**, 7369–7402 (2019).
39. Y. Rosenthal, B. K. Linsley, D. W. Oppo, Pacific ocean heat content during the past 10,000 years. *Science* **342**, (2013).

40. P. N. DiNezio, A. Timmermann, J. E. Tierney, F.-F. Jin, B. Otto-Bliesner, N. Rosenbloom, B. Mapes, R. Neale, R. F. Ivanovic, A. Montenegro, The climate response of the Indo-Pacific warm pool to glacial sea level. *Paleoceanography* **31**, 866–894 (2016).
41. A. C. Clement, R. Seager, M. A. Cane, Orbital controls on the El Niño/Southern Oscillation and the tropical climate. *Paleoceanography* **14**, 441–456 (1999).
42. A. Koutavas, S. Joanides, El Niño–Southern Oscillation extrema in the Holocene and Last Glacial Maximum. *Paleoceanography* **27**, PA4208 (2012).
43. R. Xie, F.-F. Jin, Two leading ENSO modes and El Niño types in the Zebiak-Cane model. *J. Climate* **31**, 1943–1962 (2018).
44. M. Carré, J. P. Sachs, S. Purca, A. J. Schauer, P. Braconnot, R. A. Falcón, M. Julien, D. Lavallée, Holocene history of ENSO variance and asymmetry in the eastern tropical Pacific. *Science* **345**, 1252220 (2014).
45. A. V. Fedorov, S. G. Philander, Is El Nino Changing? *Science* **288**, 1997–2002 (2000).
46. S. A. Marcott, J. D. Shakun, P. U. Clark, A. C. Mix, A reconstruction of regional and global temperature for the past 11,300 years. *Science* **339**, 1198–1201 (2013).
47. J. Laskar, P. Robutel, F. Joutel, M. Gastineau, A. C. M. Correia, B. Levrard, A long-term numerical solution for the insolation quantities of the Earth. *Astron. Astrophys.* **428**, 261–285 (2004).
48. J. D. Shakun, P. U. Clark, F. He, S. A. Marcott, A. C. Mix, Z. Liu, B. Ottoa-Bliesner, A. Schmittner, E. Bard, Global warming preceded by increasing carbon dioxide concentrations during the last deglaciation. *Nature* **484**, 49–54 (2012).
49. L. E. Lisiecki, M. E. Raymo, A Pliocene-Pleistocene stack of 57 globally distributed benthic $\delta^{18}O$ records. *Paleoceanography* **20**, PA1003 (2005).
50. J. Yu, R. F. Anderson, Z. Jin, J. W. B. Rae, B. N. Opdyke, S. M. Eggins, Responses of the deep ocean carbonate system to carbon reorganization during the Last Glacial-interglacial cycle. *Quat. Sci. Rev.* **76**, 39–52 (2013).
51. W. Fan, Z. Jian, Z. Chu, H. Dang, Y. Wang, F. Bassinot, X. Han, Y. Bian, Variability of the Indonesian Throughflow in the Makassar Strait over the Last 30 ka. *Sci. Rep.* **8**, 5678 (2018).
52. P. Anand, H. Elderfield, M. H. Conte, Calibration of Mg/Ca thermometry in planktonic foraminifera from a sediment trap time series. *Paleoceanography* **18**, 1050 (2003).
53. Y. Rosenthal, S. Perron-Cashman, C. H. Lear, E. Bard, S. Barker, K. Billups, M. Bryan, M. L. Delaney, P. B. DeMenocal, G. S. Dwyer, H. Elderfield, C. R. German, M. Greaves, D. W. Lea, T. M. Marchitto Jr., D. K. Pak, G. L. Paradis, A. D. Russell, R. R. Schneider, K. Scheiderich, L. Stott, K. Tachikawa, E. Tappa, R. Thunell, M. Wara, S. Weldeab, P. A. Wilson, Interlaboratory comparison study of Mg/Ca and Sr/Ca measurements in planktonic foraminifera for paleoceanographic research. *Geochem. Geophys. Geosyst.* **5**, Q04D09 (2004).

54. P. A. Martin, D. W. Lea, A simple evaluation of cleaning procedures on fossil benthic foraminiferal Mg/Ca. *Geochem. Geophys. Geosyst.* **3**, 8401 (2002).
55. S. Barker, M. Greaves, H. Elderfield, A study of cleaning procedures used for foraminiferal Mg/Ca paleothermometry. *Geochem. Geophys. Geosyst.* **4**, 8407 (2003).
56. J. F. Schröder, A. Holbourn, W. Kuhnt, K. Küssner, Variations in sea surface hydrology in the southern Makassar Strait over the past 26 kyr. *Quat. Sci. Rev.* **154**, 143–156 (2016).
57. A. Y. Sadekov, R. Ganeshram, L. Pichevin, R. Berdin, E. McClymont, H. Elderfield, A. W. Tudhope, Palaeoclimate reconstructions reveal a strong link between El Niño-Southern Oscillation and Tropical Pacific mean state. *Nat. Commun.* **4**, 2692 (2013).
58. L. D. Pena, I. Cacho, P. Ferretti, M. A. Hall, El Niño–Southern Oscillation–like variability during glacial terminations and interlatitudinal teleconnections. *Paleoceanography* **23**, PA3101 (2008).
59. M. Yamamoto, R. Suemune, T. Oba, Equatorward shift of the subarctic boundary in the northwestern Pacific during the last deglaciation. *Geophys. Res. Lett.* **32**, L05609 (2005).
60. B. E. Bemis, H. J. Spero, J. Bijma, D.W. Lea, Reevaluation of the oxygen isotopic composition of planktonic foraminifera: Experimental results and revised paleotemperature equations. *Paleoceanography* **13**, 150–160 (1998).
61. J. Jouzel, V. Masson-Delmotte, O. Cattani, G. Dreyfus, S. Falourd, G. Hoffmann, B. Minster, J. Nouet, J.-M. Barnola, J. Chappellaz, H. Fischer, J. C. Gallet, S. Johnsen, M. Leuenberger, L. Loulergue, D. Luethi, H. Oerter, F. Parrenin, G. Raisbeck, D. Raynaud, A. Schilt, J. Schwander, E. Selmo, R. Souchez, R. Spahni, B. Stauffer, J. P. Steffensen, B. Stenni, T. F. Stocker, J. L. Tison, M. Werner, E. W. Wolff, Orbital and millennial antarctic climate variability over the past 800,000 years. *Science* **317**, 793–796 (2007).
62. E. J. Steig, E. J. Brook, J. W. C. White, C. M. Sucher, M. L. Bender, S. J. Lehman, D. L. Morse, E. D. Waddington, G. D. Clow, Synchronous climate changes in antarctica and the north atlantic. *Science* **282**, 92–95 (1998).
63. A. E. Shevenell, A. E. Ingalls, E. W. Domack, C. Kelly, Holocene Southern Ocean surface temperature variability west of the Antarctic Peninsula. *Nature* **470**, 250–254 (2011).
64. Y. J. Wang, H. Cheng, R. L. Edward, Z. S. An, J. Y. Wu, C.-C. Shen, J. A. Dorale, A high-resolution absolute-dated late pleistocene monsoon record from Hulu Cave, China. *Science* **294**, 2345–2348 (2001).
65. C. A. Dykoski, R. L. Edwards, H. Cheng, D. Yuan, Y. Cai, M. Zhang, Y. Lin, J. Qing, Z. An, J. Revenaugh, A high-resolution, absolute-dated Holocene and deglacial Asian monsoon record from Dongge Cave, China. *Earth Planet. Sci. Lett.* **233**, 71–86 (2005).

66. J. W. Partin, K. M. Cobb, J. F. Adkins, B. Clark, D. P. Fernandez, Millennial-scale trends in west Pacific warm pool hydrology since the Last Glacial Maximum. *Nature* **449**, 452–455 (2007).
67. A. Timmermann, S. J. Lorenz, S.-I. An, A. Clement, S.-P. Xie, The effect of orbital forcing on the mean climate and variability of the tropical Pacific. *J. Clim.* **20**, 4147–4159 (2007).
68. W. Fan, Z. Jian, F. Bassinot, Z. Chu, Holocene centennial-scale changes of the Indonesian and South China Sea throughflows: Evidences from the Makassar Strait. *Global Planet. Change* **111**, 111–117 (2013).
69. H. Dang, Z. Jian, C. Kissel, F. Bassinot, Precessional changes in the western equatorial Pacific hydroclimate: A 240 kyr marine record from the Halmahera Sea, East Indonesia, *Geochem. Geophys. Geosyst.* **16**, 148–164 (2015).
70. A. Holbourn, W. Kuhnt, J. Xu, Indonesian Throughflow variability during the last 140 ka: The Timor Sea outflow. *Geol. Soc. Spec. Publ.* **355**, 283–303 (2011).
71. H. Dang, J. Wu, Z. Xiong, P. Qiao, T. Li, Z. Jian, Orbital and sea-level changes regulate the iron-associated sediment supplies from Papua New Guinea to the equatorial Pacific. *Quat. Sci. Rev.* **239**, 106361 (2020).
72. Y. Rosenthal, D. W. Oppo, B. K. Linsley, The amplitude and phasing of climate change during the last deglaciation in the Sulu Sea, western equatorial Pacific. *Geophys. Res. Lett.* **30**, 1428 (2003).
73. L. Stott, A. Timmermann, R. Thunell, Southern Hemisphere and deep-sea warming led deglacial atmospheric CO_2 rise and tropical warming. *Science* **318**, 435–438 (2007).
74. K. Visser, R. Thunell, L. Stott, Magnitude and timing of temperature change in the Indo-Pacific warm pool during deglaciation. *Nature* **421**, 152–155 (2003).
75. C. Levi, L. Labeyrie, F. Bassinot, F. Guichard, E. Cortijo, C. Waelbroeck, N. Caillon, J. Duprat, T. de Garidel-Thoron, H. Elderfield, Low-latitude hydrological cycle and rapid climate changes during the last deglaciation. *Geochem. Geophys. Geosyst.* **8**, Q05N12 (2007).
76. F. T. Gibbons, D. W. Oppo, M. Mohtadi, Y. Rosenthal, J. Cheng, Z. Liu, B. K. Linsley, Deglacial $\delta^{18}O$ and hydrologic variability in the tropical Pacific and Indian Oceans. *Earth Planet. Sci. Lett.* **387**, 240–251 (2014).
77. M. Hendrizan, W. Kuhnt, A. Holbourn, Variability of Indonesian Throughflow and Borneo runoff during the last 14 kyr. *Paleoceanography* **32**, 1054–1069 (2017).
78. R. Y. Setiawan, M. Mohtadi, J. Southon, J. Groeneveld, S. Steinke, D. Hebbeln, The consequences of opening the Sunda Strait on the hydrography of the eastern tropical Indian Ocean. *Paleoceanography* **30**, 1358–1372 (2015).
79. M. Mohtadi, A. Lückge, S. Steinke, J. Groeneveld, D. Hebbeln, N. Westphal, Late Pleistocene surface and thermocline conditions of the eastern tropical Indian Ocean. *Quat. Sci. Rev.* **29**, 887–896 (2010).
80. M. Mohtadi, M. Prange, D. W. Oppo, R. De Pol-Holz, U. Merkel, X. Zhang, S. Steinke, A. Lückge, North Atlantic forcing of tropical Indian Ocean climate. *Nature* **509**, 76–80 (2014).